A Conceptual Introduction to Hamiltonian Monte Carlo

Michael Betancourt

Abstract. Hamiltonian Monte Carlo has proven a remarkable empirical success, but only recently have we begun to develop a rigorous understanding of why it performs so well on difficult problems and how it is best applied in practice. Unfortunately, that understanding is confined within the mathematics of differential geometry which has limited its dissemination, especially to the applied communities for which it is particularly important.

In this review I provide a comprehensive conceptual account of these theoretical foundations, focusing on developing a principled intuition behind the method and its optimal implementations rather of any exhaustive rigor. Whether a practitioner or a statistician, the dedicated reader will acquire a solid grasp of how Hamiltonian Monte Carlo works, when it succeeds, and, perhaps most importantly, when it fails.

Michael Betancourt is a research scientist in the Applied Statistics Center at Columbia University. Much of this review was completed as a Research Fellow at the Centre for Research in Statistical Methodology, University of Warwick, Coventry CV4 7AL, UK (e-mail: betanalpha@gmail.com).

CONTENTS

Hamiltonian Monte Carlo has followed a long and winding path into modern statistical computing. The method was originally developed in the late 1980s as *Hybrid Monte Carlo* to tackle calculations in Lattice Quantum Chromodynamics (Duane et al., 1987), a field focused on understanding the structure of the protons and neutrons that comprise nuclei, atoms, and ultimately the world around us. Within a few years Radford Neal recognized the potential of the method for problems in applied statistics in his pioneering work on Bayesian neural networks (Neal, 1995). Over the next decade the method began to make appearances in textbooks, notably MacKay (2003), who first used the term Hamiltonian Monte Carlo instead of Hybrid Monte Carlo, and Bishop (2006). Neal's influential review (Neal, 2011), however, really introduced the approach into the mainstream of statistical computing. With the rise of high-performance software implementations such as Stan (Stan Development Team, 2017), the method has now become a pervasive tool across many scientific, medical, and industrial applications.

Only recently, however, have we begun to understand why the success of Hamiltonian Monte Carlo has been so extensive. Instead of relying on fragile heuristics, the method is built upon a rich theoretical foundation that makes it uniquely suited to the high-dimensional problems of applied interest (Betancourt et al., 2014). Unfortunately, this theoretical foundation is formulated in terms of differential geometry, an advanced field of mathematics that is rarely included in statistical pedagogy. Consequently this formal construction is often out of reach of theoretical and applied statisticians alike.

The aim of this paper is to introduce the intuition behind the success of Hamiltonian Monte Carlo while avoiding the mathematical details; in particular, I assume only a basic familiarity with probability and calculus. Such an approach necessarily sacrifices rigor, but I hope the concepts will be sufficiently intuitive to satisfy readers working in applied fields. I highly encourage those interested in learning more about Hamiltonian Monte Carlo, or even contributing to its development, to follow up on the references discussed in Betancourt et al., 2014, Section 2.

Our story will begin with an introduction to the geometry of high-dimensional probability distributions and how that geometry frustrates efficient statistical computing. We will then consider Markov chain Monte Carlo from this geometric perspective, motiving the features necessary to scale the approach to such high-dimensional problems. By developing a method that inherently satisfies these criteria we will very naturally be led to Hamiltonian Monte Carlo. Finally I will discuss how this understanding can be extended to motivate not just the method itself but also its efficient practical implementation, including optimized tuning as well as inherent diagnostics of pathological behavior.

1. COMPUTING EXPECTATIONS BY EXPLORING PROBABILITY DISTRIBUTIONS

The ultimate undertaking in statistical computing is evaluating expectations with respect to some distinguished *target* probability distribution. For example, we might be interested in extracting information from a posterior distribution over model configuration space in

Bayesian inference, or computing coverage of an estimator with respect to the likelihood over data space in frequentist statistics. Here we will be agnostic, considering only a target distribution, π, on a D-dimensional sample space, Q, and the corresponding expectations of functions, $\mathbb{E}_\pi[f]$.

Probability distributions, and the corresponding expectations, are rather abstract objects, however, and if we want to use them in practice then we need a more explicit means of specifying them. Here we will assume that the sample space is smooth, in which case that we can represent the target distribution with a *probability density function* and expectations as integrals. Care must be taken, however, as this representation hides some of the more subtle behaviors of high-dimensional spaces that are critical towards understanding how to compute these integrals, and hence the desired expectations, efficiently.

1.1 Computing Expectations in Practice

We begin by assuming that the target sample space, Q, can be parameterized by the real numbers such that every point $q \in Q$ can be specified with D real numbers. Given a parameter space, $\mathcal{Q}$, we can then specify the target distribution as a smooth probability density function, $\pi(q)$, while expectations reduce to integrals over parameter space,

$$\mathbb{E}_\pi[f] = \int_{\mathcal{Q}} \mathrm{d}q \, \pi(q) \, f(q) \, .$$

Parameterizations are not unique: we can always take another parameterization, $\mathcal{Q}'$, over which we specify the target distribution with a different probability density function, $\pi'(q')$, while expectations reduce to the new integral,

$$\mathbb{E}_\pi[f] = \int_{\mathcal{Q}'} \mathrm{d}q' \, \pi(q') f(q').$$

Critically, however, the expectations values themselves are invariant to any particular choice of parameterization, so the integrals must be equal,

$$\mathbb{E}_\pi[f] = \int_{\mathcal{Q}} \mathrm{d}q \, \pi(q) f(q) = \int_{\mathcal{Q}'} \mathrm{d}q' \, \pi'(q') f(q').$$

In this review we will consider only a single parameterization for computing expectations, but we must be careful to ensure that any such computation does not depend on the irrelevant details of that parameterization, such as the particular shape of the probability density function.

Once we have chosen a parameterization, the abstract expectation becomes the concrete integral. Unfortunately, for any nontrivial target distribution we will not be able to evaluate these integrals analytically, and we must instead resort to numerical methods which only *approximate* them. The accuracy of these approximations, and hence the utility of any given algorithm, however, is limited by our finite computational power.

For a method to scale to the complex problems at the frontiers of applied statistics, it has to make effective use of each and every evaluation of the target density, $\pi(q)$, and relevant functions, $f(q)$. Optimizing these evaluations is a subtle problem frustrated by the natural geometry of probability distributions, especially over high-dimensional parameter spaces.

1.2 Parsimonious Expectation Computation

One way to ensure computational *inefficiency* is to waste computational resources evaluating the target density and relevant functions in regions of parameter space that have negligible contribution to the desired expectation. In order to avoid these regions, and focus our computation only on significant regions of parameter space, we first need to identify how the target density and target function contribute to the overall expectation.

Because integration is a linear operation, scaling the integrand proportionately scales the integral. Consequently, a common intuition is to focus on regions where the integrand is largest. This intuition suggests that we consider regions where the target density and target function take on their largest values.

In practice we often are interested in computing expectations with respect to many target functions, for example in Bayesian inference we typically summarize our uncertainty with both means and variances, or multiple quantiles. Any method that depends on the specific details of any one function will then have to be repeatedly adjusted for each new function we encounter, expanding a single computational problem into many. Consequently, from here on in we will assume that any relevant function is sufficiently uniform in parameter space that its variation does not strongly effect the integrand. Keep in mind, however, that if only a single expectation is in fact of interest then exploiting the structure of that function can provide significant improvements (Mira, Solgi and Imparato, 2013; Oates, Girolami and Chopin, 2016).

This assumption implies that the variation in the integrand is dominated by the target density, and hence we should consider the neighborhood around the mode where the density is maximized. This intuition is consistent with the many statistical methods that utilize the mode, such as maximum likelihood estimators and Laplace approximations, although conflicts with our desire to avoid the specific details of the target density. Indeed, this intuition is fatally naive as it misses a critical detail.

Expectation values are given by accumulating the integrand over a *volume* of parameter space and, while the density is largest around the mode, there is not much volume there. To identify the regions of parameter space that dominate expectations we need to consider the behavior of both the density and the volume. In high-dimensional spaces the volume behaves very differently from the density, resulting in a tension that concentrates the significant regions of parameter space away from either extreme.

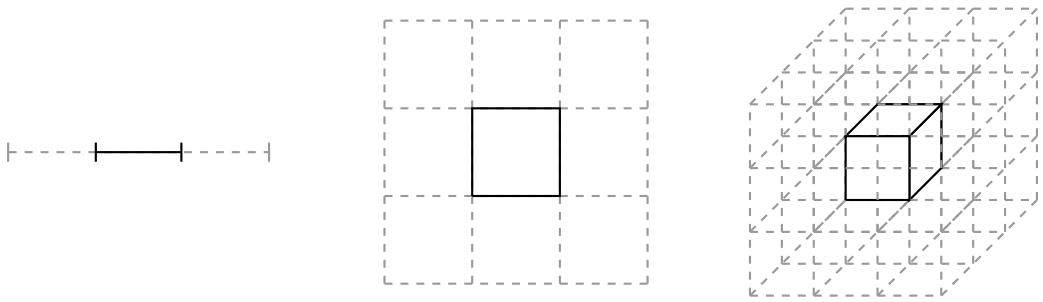

(a) (b) (c)

FIG 1. *To understand how the distribution of volume behaves with increasing dimension we can consider a rectangular partitioning centered around a distinguished point, such as the mode. (a) In one dimension the relative weight of the center partition is* $1/3$*, (b) in two dimensions it is* $1/9$*, (c) and in three dimensions it is only* $1/27$*. Very quickly the volume in the center partition becomes negligible compared to the neighboring volume.*

1.3 The Geometry of High-Dimensional Spaces

One of the characteristic properties of high-dimensional spaces is that there is much more volume outside any given neighborhood than inside of it. Although this may at first appear strange, we can build intuition to demystify this behavior by considering a few simple cases.

For example, consider partitioning parameter space into rectangular boxes centered around the mode (Figure 1). In one dimension there are only two partitions neighboring the center partition, leaving a significant volume around the mode. Adding one more dimension, however, introduces eight neighboring partitions, and in three dimensions there are already 26. In general there are $3^D - 1$ neighboring partitions in a D-dimensional space, and for even small D the volume neighboring the mode dominates the volume immediately around the mode. This pattern only amplifies if we consider more partitions further away from the mode that multiply even faster.

Alternatively, we can take a spherical view of parameter space and consider the relative volume a distance δ inside and outside of a spherical shell (Figure 2). In one dimension the interior and exterior volumes are equal, but in two and three dimensions more and more volume concentrates on the outside of the shell. Centering the shell at the mode we can see once again that the volume in any neighborhood containing the mode becomes more and more negligible as the dimension of the parameter space increases.

Generically, then, volume is largest out in the *tails* of the target distribution away from the mode, and this disparity grows exponentially with the dimension of parameter space. Consequently, the massive volume over which we integrate can compensate to give a significant contribution to the target expectation despite the smaller density. In order

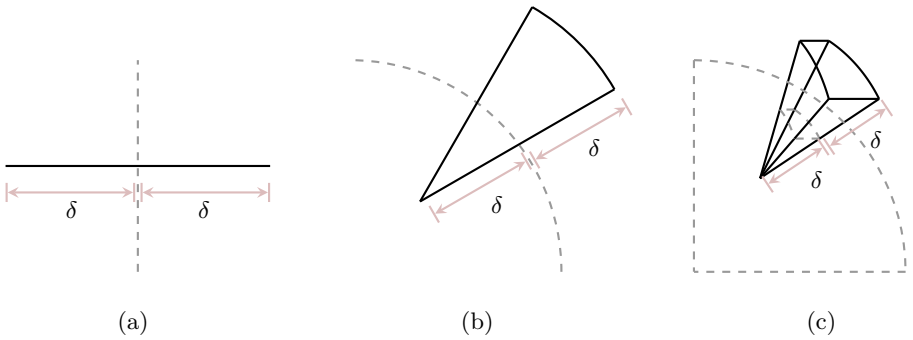

FIG 2. *The dominance of volume away from any point in parameter space can also be seen from a spherical perspective, where we consider the volume contained radial distance δ both interior to and exterior to a D-dimensional spherical shell, shown here with dashed lines. (a) In one dimension the spherical shell is a line and volumes interior and exterior are equivalent. (b) In two dimensions the spherical shell becomes circle and there is more volume immediately outside the shell than immediately inside. (c) The exterior volume grows even larger relative to the interior volume in three dimensions, where the spherical shell is now a the surface of a sphere. In fact, with increasing dimension the exterior volume grows exponentially large relative to the interior volume, and very quickly the volume around the mode is dwarfed by the volume away from the mode.*

to identify the neighborhoods that most contribute to expectations, we need to carefully balance the behavior of both the density and the volume.

1.4 The Geometry of High-Dimensional Probability Distributions

The neighborhood immediately around the mode features large densities, but in more than a few dimensions the small volume of that neighborhood prevents it from having much contribution to any expectation. On the other hand, the complimentary neighborhood far away from the mode features a much larger volume, but the vanishing densities lead to similarly negligible contributions expectations. The only significant contributions come from the neighborhood between these two extremes known as the *typical set* (Figure 3). Importantly, because probability densities and volumes transform oppositely under any reparameterization, the typical set is an invariant object that does not depend on the irrelevant details of any particular choice of parameters.

As the dimension of parameter space increases, the tension between the density and the volume grows and the regions where the density and volume are both large enough to yield a significant contribution becomes more and more narrow. Consequently the typical set becomes more singular with increasing dimension, a manifestation of *concentration of measure*. The immediate consequence of concentration of measure is that the only significant contributions to any expectation come from the typical set; evaluating the integrand outside of the typical set has negligible effect on expectations and hence is a waste of precious computational resources. In other words, we can accurately estimate expectations by

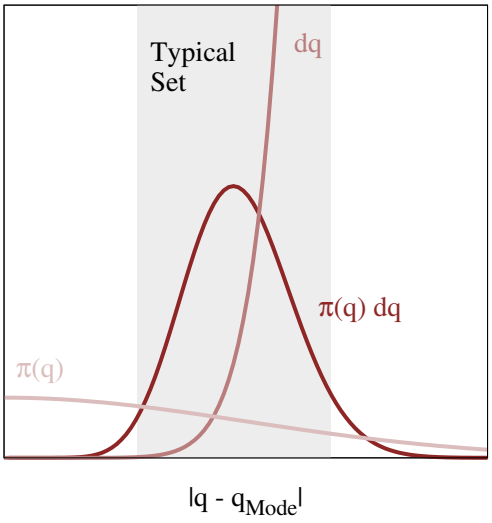

FIG 3. *In high dimensions a probability density, $\pi(q)$, will concentrate around its mode, but the volume over which we integrate that density, $\mathrm{d}q$, is much larger away from the mode. Contributions to any expectation are determined by the product of density and volume, $\pi(q)\,\mathrm{d}q$, which then concentrates in a nearly-singular neighborhood called the typical set (grey).*

averaging over the typical set instead of the entirety of parameter space. Consequently, in order to compute expectations efficiently, we have to be able to identify, and then focus our computational resources into, the typical set (Figure 4).

This helps to explain, for example, why brute force methods like naive quadrature scale so poorly with dimension. A grid of length N distributed uniformly in a D-dimensional parameter space requires N^D points and hence N^D evaluations of the integrand. Unless N is incredibly large, however, it is unlikely that any of these points will intersect the narrow typical set, and the exponentially-growing cost of averaging over the grid yields worse and worse approximations to expectations. In general, framing algorithms by how they quantify the typical set is a powerful way to quickly intuit how an algorithm will perform in practice.

Of course, understanding *why* we want to focus on the typical set in only the first step. *How* to construct an algorithm that can quantify the typical set of an arbitrary target distribution is another problem altogether. There are many strategies for this task, but one of the most generic, and hence most useful in applied practice, is *Markov chain Monte Carlo* (Robert and Casella, 1999; Brooks et al., 2011).

2. MARKOV CHAIN MONTE CARLO

Markov chain Monte Carlo uses a Markov chain to stochastically explore the typical set, generating a random grid across the region of high probability from which we can con-

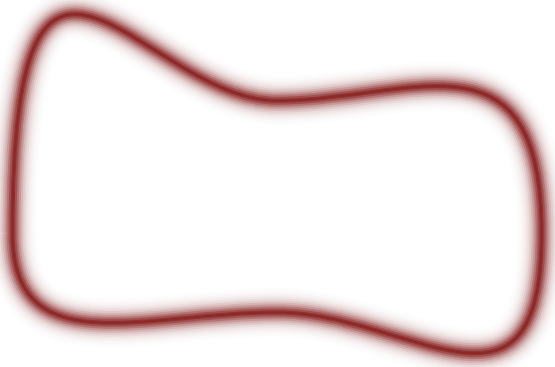

FIG 4. *In high-dimensional parameter spaces probability mass, $\pi(q)\,\mathrm{d}q$, and hence the dominant contributions to expectations, concentrates in a neighborhood called the* typical set. *In order to accurately estimate expectations we have to be able to identify where the typical set lies in parameter space so that we can focus our computational resources where they are most effective.*

struct accurate expectation estimates. Given sufficient computational resources a properly designed Markov chain will *eventually* explore the typical set of any distribution. The more practical, and much more challenging question, however, is whether a given Markov chain will explore a typical set in the finite time available in a real analysis.

In this section I'll introduce a more substantial definition of Markov chain Monte Carlo and discuss both its ideal and pathological behaviors. Finally we'll consider how to implement Markov chain Monte Carlo in practice and see how fragile of an endeavor it can be.

2.1 Estimating Expectations with Markov Chains

A *Markov chain* is a progression of points in parameter space generated by sequentially applying a random map known as a *Markov transition*. Alternatively, we can think of a Markov transition as a conditional probability density, $\mathbb{T}(q' \mid q)$, defining to which point, q', we are most likely to jump from the initial point, q (Figure 5).

An arbitrary Markov chain will simply wander through parameter space and will not be of any particular use in computing expectations. Something very special happens, however, if the Markov transition *preserves* the target distribution,

$$\pi(q) = \int_{\mathcal{Q}} \mathrm{d}q' \, \pi(q') \, \mathbb{T}(q \mid q').$$

More intuitively, this condition implies that if we generated a ensemble of samples from the target distribution and applied the transition then we would get a new ensemble that was still distributed according to the target distribution.

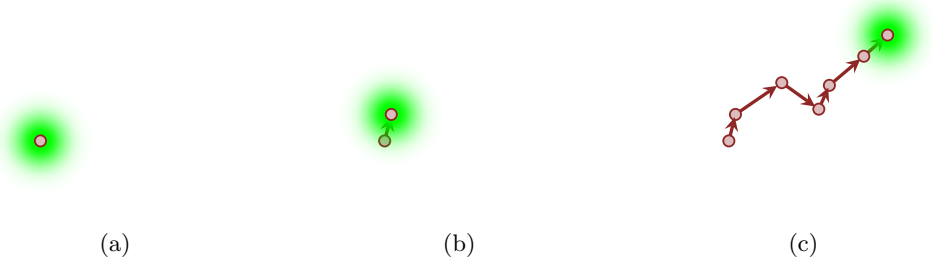

(a) (b) (c)

FIG 5. *(a) A Markov chain is a sequence of points in parameter space generated by a Markov transition density (green) that defines the probability of a new point given the current point. (b) Sampling from that distribution yields a new state in the Markov chain and a new distribution from which to sample. (c) Repeating this process generates a Markov chain that meanders through parameter space.*

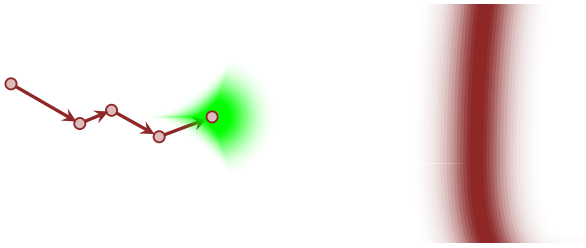

FIG 6. *When a Markov transition (green) preserves the target distribution, it concentrates towards the typical set (red), no matter where it is applied. Consequently, the resulting Markov chain will drift into and then across the typical set regardless of its initial state, providing a powerful quantification of the typical set from which we can derive accurate expectation estimators.*

So long as this condition holds, at every initial point the Markov transition will concentrate *towards* the typical set. Consequently, no matter where we begin in parameter space the corresponding Markov chain will eventually drift into, and then across, the typical set (Figure 6).

Given sufficient time, the history of the Markov chain, $\{q_0, \ldots, q_N\}$, denoted *samples* generated by the Markov chain, becomes a convenient quantification of the typical set. In particular, we can estimate expectations across the typical set, and hence expectations across the entire parameter space, by averaging the target function over this history,

$$\hat{f}_N = \frac{1}{N} \sum_{n=0}^{N} f(q_n) \,.$$

As we run the Markov chain for longer and longer, it will better explore the typical set and, up to some technicalities, these *Markov chain Monte Carlo estimators* will converge

to the true expectations,

$$\lim_{N \to \infty} \hat{f}_N = \mathbb{E}_\pi[f] \,.$$

Unfortunately, this asymptotic behavior is of limited use in practice because we do not have the infinite computational resources to ensure that we can always run a Markov chain long enough to achieve sufficient exploration. In order to develop a robust tool we need to understand how Markov chains behave after only a finite number of transitions.

2.2 Ideal Behavior

Under ideal conditions, Markov chains explore the target distribution in three distinct phases. In the first phase the Markov chain converges towards the typical set from its initial position in parameter space while the Markov chain Monte Carlo estimators suffer from strong biases (Figure 7a). The second phase begins once the Markov chain finds the typical set and persists through the first sojourn across the typical set. This initial exploration is extremely effective and the accuracy of Markov chain Monte Carlo estimators rapidly improves as the bias from the initial samples is eliminated (Figure 7b). The third phase consists of all subsequent exploration where the Markov chain refines its exploration of the typical set and the precision of the Markov chain Monte Carlo estimators improves, albeit at a slower rate (Figure 7c).

Once the Markov chain has entered into this third phase the Markov chain Monte Carlo estimators satisfy a Central Limit Theorem

$$\hat{f}_N^{\text{MCMC}} \sim \mathcal{N}(\mathbb{E}_\pi[f], \text{MCMC-SE}) \,,$$

where the *Markov Chain Monte Carlo Standard Error* is given by

$$\text{MCMC-SE} \equiv \sqrt{\frac{\text{Var}_\pi[f]}{\text{ESS}}}.$$

The *effective sample size* is defined as

$$\text{ESS} = \frac{N}{1 + 2 \sum_{l=1}^{\infty} \rho_l},$$

where ρ_l is the lag-l autocorrelation of f over the history of the Markov chain. The effective sample size quantifies the number of exact samples from the target distribution necessary to give an equivalent estimator precision and hence the effective number of exact samples "contained" in the Markov chain; we can also interpret the effective sample size as the total number of sojourns the Markov chain has made across the typical set. In practice the effective sample size can be estimated from the Markov chain itself, although care must be taken to avoid biases (Geyer, 1992; Gelman et al., 2014).

Because the states of the Markov chain generated during the initial convergence phase mostly bias Markov chain Monte Carlo estimators, we can drastically improve the precision

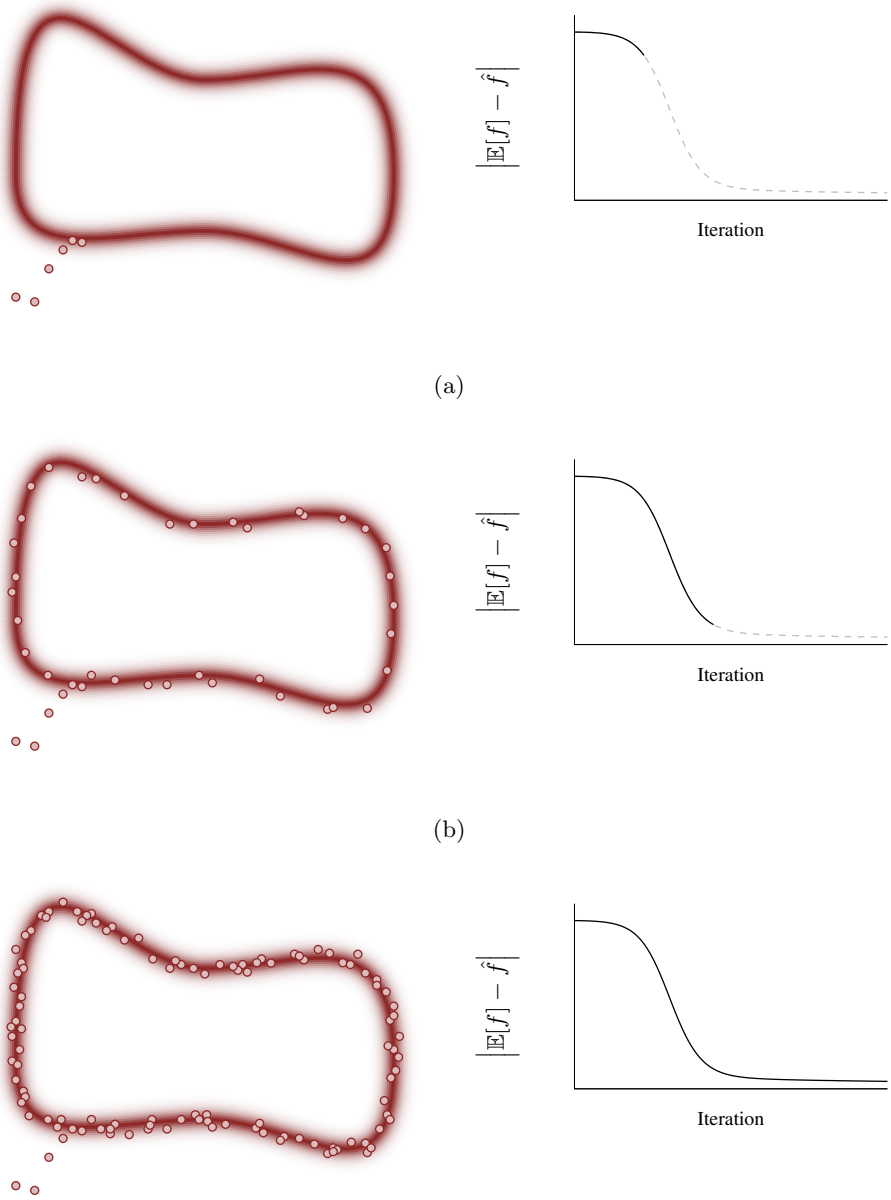

FIG 7. *Under ideal circumstances, a Markov chain explores the target distribution in three phases. (a) First the Markov chain converges to the typical set and estimators suffer from initial but ultimately transient biases. (b) Once the Markov chain finds the typical set and makes the first sojourn through it, this initial bias rapidly vanishes and the estimators become much more accurate. (c) As the Markov chain continues it explores more details of the typical set, gradually reducing the precision of the Markov chain Monte Carlo estimators towards zero.*

FIG 8. *Markov chains typically have trouble exploring regions of the typical set with large curvature (green). Incomplete exploration biases Markov chain Monte Carlo estimators and spoils critical results such as Central Limit Theorems.*

of these estimators by using only those samples generated once the Markov chain has begun to explore the typical set. Consequently, it is common practice to *warm up* the Markov chain by throwing away those initial converging samples before computing Markov chain Monte Carlo estimators. Warm-up can also be extended to allow for any degrees of freedom in the Markov transition to be empirically optimized without biasing the subsequent estimators.

2.3 Pathological Behavior

Unfortunately, this idealized behavior requires that the Markov transition is compatible with the structure of the target distribution. When the target distribution exhibits pathological behavior, however, Markov transitions will have trouble exploring and Markov chain Monte Carlo will fail.

Consider, for example, a target probability distribution where the typical set pinches into a region of high curvature (Figure 8). Most Markov transitions are not able to resolve these details and hence they cannot maneuver into these tight regions. The resulting Markov chains simply ignore them, biasing subsequent Markov chain Monte Carlo estimators due to the incomplete exploration. It is as if there are thin but deep cracks across a surface in parameter space hiding a significant amount of probability that the Markov chains pass right over and miss entirely.

Because Markov chains have to recover the exact expectations asymptotically, they have to somehow compensate for not being able to explore these regions. Typically the Markov chain accomplishes this by getting stuck near the boundary of the pathological region: as the chain hovers around the pathological region the estimators are drawn down almost as if the Markov chain were exploring the pathological region. Eventually this causes the estimators to overcorrect, inducing a bias in the opposite direction, at which point the Markov chain escapes to explore the rest of the typical set (Figure 9).

Ultimately this behavior results in estimators that strongly oscillate around the true expectations. Asymptotically the oscillations average out to give the true values, but that

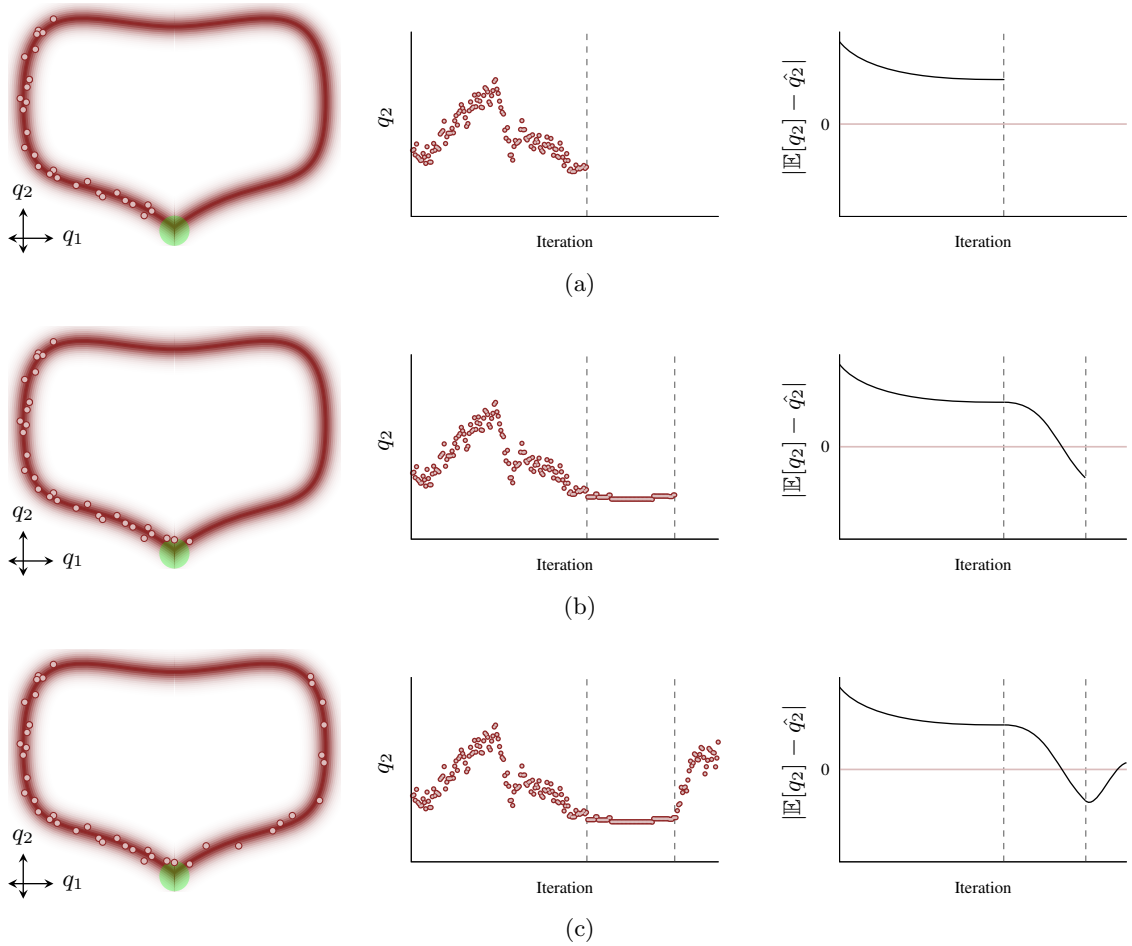

FIG 9. *In practice, pathological regions of the typical set usually cause Markov chains to get "stuck". (a) Initially the Markov chain explores well-behaved regions of the typical set, avoiding the pathological neighborhood entirely and biasing Markov chain Monte Carlo estimators. (b) If the Markov chain is run long enough then it will get stuck near the boundary of the pathological region, slowly correcting the Markov chain Monte Carlo estimators. (c) Eventually the Markov chain escapes to explore the rest of the typical set. This process repeats, causing the resulting estimators to oscillate around the true expectations and inducing strong biases unless the chain is improbably stopped at exactly the right time.*

balance is fragile. Terminating the Markov chain after only a finite time almost always destroys this balance, and resulting estimators will suffer from substantial biases.

Whether or not features of the target distribution become pathological in a given application of Markov chain Monte Carlo depends on how exactly the given Markov transition interacts with those features. Some transitions are generically more robust to certain features than others, and some can achieve robust performance by carefully tuning degrees of freedom in the transition. Regardless, great care has to be taken to ensure that a Markov transition is sufficiently robust to be used in a given application.

Formally, the sufficient condition that guarantees the idealized behavior, most importantly a Central Limit Theorem for the Markov chain Monte Carlo estimators, is known as *geometric ergodicity* (Roberts and Rosenthal, 2004). Unfortunately, geometric ergodicity is extremely difficult to verify theoretically for all but the simplest problems and we must instead resort to empirical diagnostics. The most powerful of these is the split $\hat{R}$ statistic (Gelman et al., 2014), which quantifies the variation of an ensemble of Markov chains initialized from different points in parameter space. The pathologies that frustrate geometric ergodicity induce inconsistencies amongst the individual chains in the ensemble, and hence large values of split $\hat{R}$. Consequently, when split $\hat{R}$ is not near the nominal value of 1, we should be suspicious of geometric ergodicity being satisfied and hence the practical utility of any resulting estimators.

2.4 The Metropolis-Hastings Algorithm

Given a Markov transition that targets the desired distribution, Markov chain Monte Carlo defines a generic strategy for quantifying the typical set. Constructing such a transition, however, is itself a nontrivial problem. Fortunately there are various procedures for automatically constructing appropriate transitions for any given target distribution, with the foremost amongst these the *Metropolis-Hastings* algorithm (Metropolis et al., 1953; Hastings, 1970).

The Metropolis-Hastings algorithm is comprised of two steps: a proposal and a correction. The proposal is any stochastic perturbation of the initial state while the correction rejects any proposals that stray too far away from the typical set of the target distribution. More formally, let $\mathbb{Q}(q' \mid q)$ be the probability density defining each proposal. The probability of accepting a given proposal is then given by

$$a(q' \mid q) = \min\left(1, \frac{\mathbb{Q}(q \mid q')\,\pi(q')}{\mathbb{Q}(q' \mid q)\,\pi(q)}\right).$$

The original Markov chain Monte Carlo algorithm, and one still commonly in use today, utilizes a Gaussian distribution as its proposal mechanism,

$$\mathbb{Q}(q' \mid q) = \mathcal{N}(q' \mid q, \Sigma),$$

an algorithm to which I will refer to as *Random Walk Metropolis*. Because the proposal mechanism is symmetric under the exchange of the initial and proposed points, the proposal

density cancels in the acceptance probability, leaving the simple form

$$a(q' \mid q) = \min\left(1, \frac{\pi(q')}{\pi(q)}\right).$$

Random Walk Metropolis is not only simple to implement, it also has a particularly nice intuition. The proposal distribution is biased towards large volumes, and hence the tails of the target distribution, while the Metropolis correction rejects those proposals that jump into neighborhoods where the density is too small. The combined procedure then preferentially selects out those proposals that fall into neighborhoods of high probability mass, concentrating towards the typical set as desired.

Because of its conceptual simplicity and the ease in which it can be implemented by practitioners, Random Walk Metropolis is still popular in many applications. Unfortunately, that seductive simplicity hides a performance that scales poorly with increasing dimension and complexity of the target distribution.

The geometrical perspective introduced in Section 1 proves particularly powerful in illuminating these issues. As the dimension of the target distribution increases, the volume exterior to the typical set overwhelms the volume interior to the typical set, and almost every Random Walk Metropolis proposal will produce a point on the outside of the typical set, towards the tails (Figure 10a). The density of these points, however, is so small, that the acceptance probability becomes negligible. In this case almost all of the proposals will be rejected and the resulting Markov chain will only rarely move. We can induce a larger acceptance probability by shrinking the size of the proposal to stay within the typical set (Figure 10b), but those small jumps will move the Markov chain extremely slowly.

Regardless of how we tune the covariance of the Random Walk Metropolis proposal or the particular details of the target distribution, the resulting Markov chain will explore the typical set extremely slowly in all but the lowest dimensional spaces. In the worst case this exploration will be so slow that we can't even complete a single sojourn across the typical set using our finite computational resources, and the resulting Markov chain Monte Carlo estimators will be highly biased. Even if we can safely reach the mixing regime, however, the slow exploration will yield large autocorrelations and extremely imprecise estimators.

Consequently, if want to scale Markov chain Monte Carlo to the high-dimensional probability distributions of practical interest then we need a better way of exploring the typical set. In particular, we need to better exploit the geometry of the typical set itself.

3. THE FOUNDATIONS OF HAMILTONIAN MONTE CARLO

The guess-and-check strategy of Random Walk Metropolis is doomed to fail in high-dimensional spaces where there are an exponential number of directions in which to guess but only a singular number of directions that stay within the typical set and pass the check. In order to make large jumps away from the initial point, and into new, unexplored regions of the typical set, we need to exploit information about the geometry of the typical set

(a) (b)

FIG 10. *In high dimensions, the Random Walk Metropolis proposal density (green) is strongly biased towards the outside of the typical set where the target density, and hence the Metropolis acceptance probability vanishes. (a) If the proposal variances are large then the proposals will stray too far away from the typical set and are rejected. (b) Smaller proposal variances stay within the typical set and hence are accepted, but the resulting transition density concentrates tightly around the initial point. Either way we end up with a Markov chain that explores the typical set very, very slowly.*

itself. Specifically, we need transitions that can follow those contours of high probability mass, coherently gliding through the typical set (Figure 11).

Hamiltonian Monte Carlo is the unique procedure for automatically generating this coherent exploration for sufficiently well-behaved target distributions. In this section I will first introduce some intuition to motivate how we can generate the desired exploration by carefully exploiting the differential structure of the target probability density. I will then discuss the procedure more formally, ending with the complete construction of the Hamiltonian Markov transition.

3.1 Informing Effective Markov Transitions

How can we distill the geometry of the typical set into information about how to move through it? When the sample space is continuous, a natural way of encoding this direction information is with a *vector field* aligned with the typical set (Figure 12). A vector field is the assignment of a direction at every point in parameter space, and if those directions are aligned with the typical set then they act as a guide through this neighborhood of largest target probability.

In other words, instead of fumbling around parameter space with random, uninformed jumps, we can follow the direction assigned to each at point for a small distance. By construction this will move us to a new point in the typical set, where we will find a new direction to follow. Continuing this process traces out a coherent trajectory through the typical set that efficiently moves us far away from the initial point to new, unexplored regions of the typical set as quickly as possible.

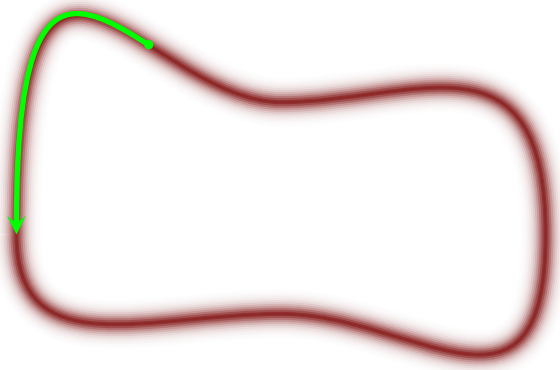

FIG 11. *Most Markov transitions are diffusive, concentrating around the initial point such that the corresponding Markov chains linger in small neighborhoods of the typical set for long periods of time. In order to maximize the utility of our computational resources we need* coherent *Markov transitions that are able to glide across the typical set towards new, unexplored neighborhoods.*

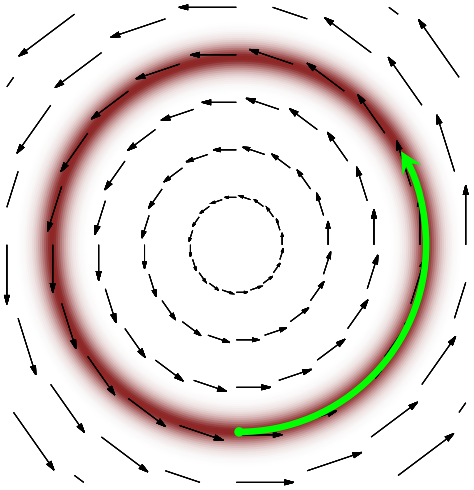

FIG 12. *A vector field is the assignment of a direction at every point in parameter space. When those directions are aligned with the typical set we can follow them like guide posts, generating coherent exploration of the target distribution.*

We are still left, however, with the problem of constructing a vector field aligned with the typical set using only information that we can extract from the target distribution. The natural information that we have yet to exploit is the differential structure of the target distribution which we can query through the *gradient* of the target probability density function. In particular, the gradient defines a vector field in parameter space sensitive to the structure of the target distribution (Figure 13).

Unfortunately, that sensitivity is not sufficient as the gradient will never be aligned with the typical set. Following the guidance of the gradient pulls us away from the typical set and towards the mode of the target density. This behavior, however, isn't necessarily surprising. Because the target density depends on the choice of parameterization, so too will its gradient. Consequently the gradient can direct us towards only parameterization-sensitive neighborhoods like that around the mode, and not the parameterization-invariant neighborhoods within the typical set.

To utilize the information in the gradient we need to complement it with additional geometric constraints, carefully removing the dependence on any particular parameterization while twisting the directions to align with the typical set. Auspiciously, there is an elegant procedure for doing exactly this in a field of mathematics known as differential geometry. Because differential geometry is a challenging subject that is rarely taught in applied statistics curricula, however, building an understanding of the details and subtleties of that procedure is no easy task.

Fortunately, there is a convenient equivalence that we can employ to build an intuition

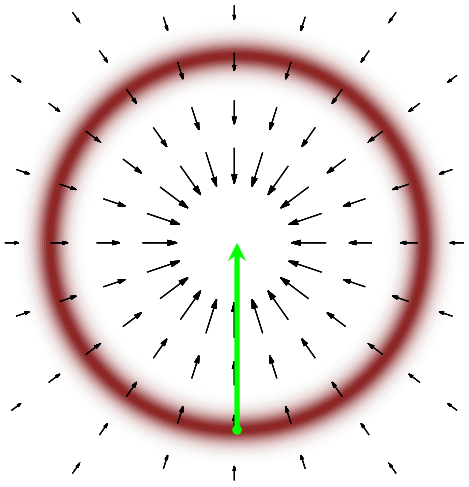

FIG 13. *The gradient of the target probability density function encodes information about the geometry of the typical set, but not enough to guide us through the typical set by itself. Following along the gradient instead pulls us away from the typical set and towards the mode of the target density. In order to generate motion through the typical set we need to introduce additional structure that carefully twists the gradient into alignment with the typical set.*

for this procedure without delving into the technical details. The same differential geometry that we need to use to correct the density gradients also happens to be the mathematics that describes classical physics. In other words, for every probabilistic system there is a mathematically equivalent *physical* system about which we can more easily reason.

For example, instead of trying to reason about a mode, a gradient, and a typical set, we can equivalently reason about a planet, a gravitational field, and an orbit (Figure 14). The probabilistic endeavor of exploring the typical set then becomes a physical endeavor of placing a satellite in a stable orbit around the hypothetical planet.

Because these are just two different perspectives of the same mathematical system, they will suffer from the same pathologies. Indeed, if we place a satellite at rest out in space it will fall in the gravitational field and crash into the surface of the planet, just as naive gradient-driven trajectories crash into the mode (Figure 15). From either the probabilistic or physical perspective we are left with a catastrophic outcome.

The physical picture, however, provides an immediate solution: although objects at rest will crash into the planet, we can maintain a stable orbit by endowing our satellite with enough *momentum* to counteract the gravitational attraction. We have to be careful, however, in how exactly we add momentum to our satellite. If we add too little momentum transverse to the gravitational field, for example, then the gravitational attraction will be too strong and the satellite will still crash into the planet (Figure 16a). On the other hand, if we add too much momentum then the gravitational attraction will be too weak to

FIG 14. *The exploration of a probabilistic system is mathematically equivalent to the exploration of a physical system. For example, we can interpret the mode of the target density as a massive planet and the gradient of the target density as that planet's gravitational field. The typical set becomes the space around the planet through which we want a test object, such as a satellite, to orbit.*

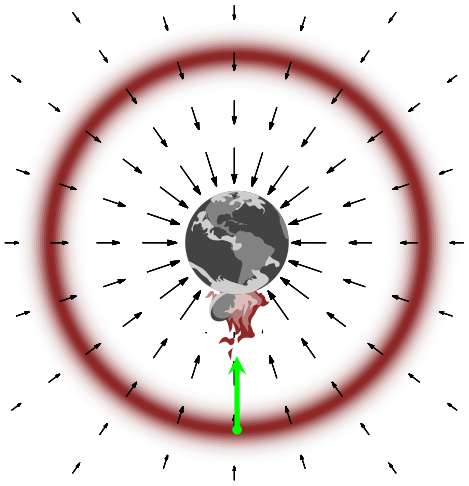

FIG 15. *The analogous physical system suffers from the same pathologies as the motivating probabilistic system. In particular, a satellite at rest will fall under the planet's gravity and crash into the surface of the planet, just as any gradient-driven trajectory will crash into the mode.*

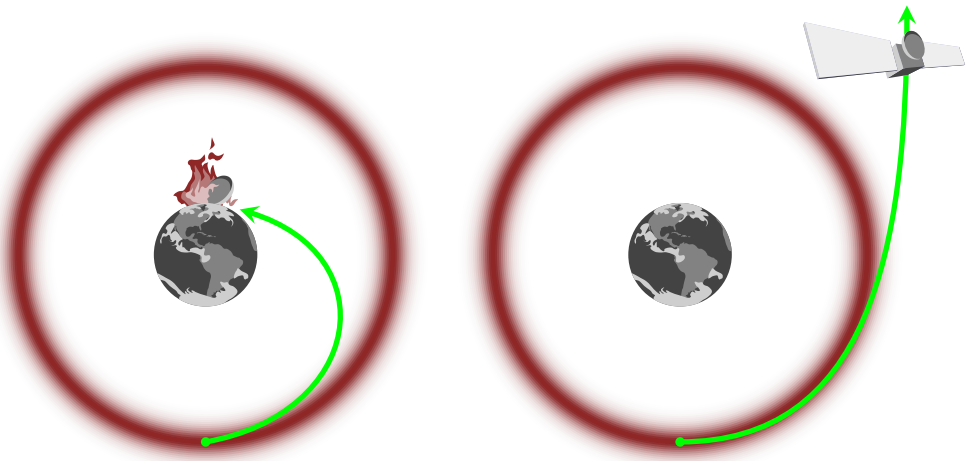

(a) (b)

FIG 16. *(a) Without enough transverse momentum to balance against the gravitational attraction of the planet, a satellite will still crash into the planet. (b) On other other hand, if the satellite is given too much momentum then the gravitational attraction will be too weak to capture the satellite in a stable orbit, which will instead abandon the planet for the depths of space.*

capture the satellite at all and it will instead fly out into the depths of space (Figure 16b).

If we add just the right amount of momentum, however, then the momentum will exactly balance against the gravitational force, and the corresponding dynamics of the system will be *conservative*. As the satellite falls towards the planet the momentum grows until it is large enough to propel the satellite away from the planet. Similarly, if the satellite drifts away from the planet then the momentum shrinks and the satellite slows, allowing gravity more time to pull it back towards the planet. This careful exchange balances along the desired orbit, ensuring that the subsequent evolution of the satellite will generate exactly the trajectories that we need (Figure 17).

Pulling this physical intuition back into the probabilistic perspective, the key to twisting the gradient vector field into a vector field aligned with the typical set, and hence one capable of generating efficient exploration, is to expand our original probabilistic system with the introduction of auxiliary momentum parameters. As in the physical system, however, we can't just add those momentum parameters arbitrarily. They need to be endowed with a probabilistic structure that ensures conservative dynamics.

Remarkably, there is only one procedure for introducing auxiliary momentum with such a probabilistic structure: Hamiltonian Monte Carlo.

3.2 Phase Space and Hamilton's Equations

Conservative dynamics in physical systems requires that volumes are exactly preserved. As the system evolves, any compression or expansion in position space must be compensated

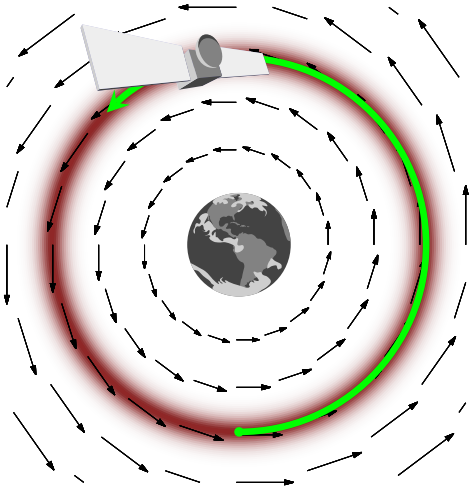

FIG 17. *When we introduce exactly the right amount of momentum to the physical system, the equations describing the evolution of the satellite define a vector field aligned with the orbit. The subsequent evolution of the system will then trace out orbital trajectories.*

with a respective expansion or compression in momentum space to ensure that the volume of any neighborhood in position-momentum *phase space* is unchanged (Figure 18).

In order to mimic this behavior in our probabilistic system we need to introduce auxiliary momentum parameters, p_n, to complement each dimension of our target parameter space,

$$q_n \to (q_n, p_n) \,,$$

expanding the D-dimensional parameter space into a $2D$-dimensional phase space. Moreover, these auxiliary momentum have to be dual to the target parameters, transforming in the opposite way under any reparameterization so that phase space volumes are invariant.

Having expanded the target parameter space to phase space, we can now lift the target distribution onto a joint probability distribution on phase space called the *canonical distribution*. We do this with the choice of a conditional probability distribution over the auxiliary momentum,

$$\pi(q, p) = \pi(p \mid q)\, \pi(q) \,,$$

which ensures that if we marginalize out the momentum we immediately recover our target distribution. More importantly, it guarantees that any trajectories exploring the typical set of the phase space distribution will project to trajectories exploring the typical set of the target distribution (Figure 19).

Because of the duality of the target parameters and the auxiliary momentum, the corresponding probability densities also transform oppositely to each other. In particular, the

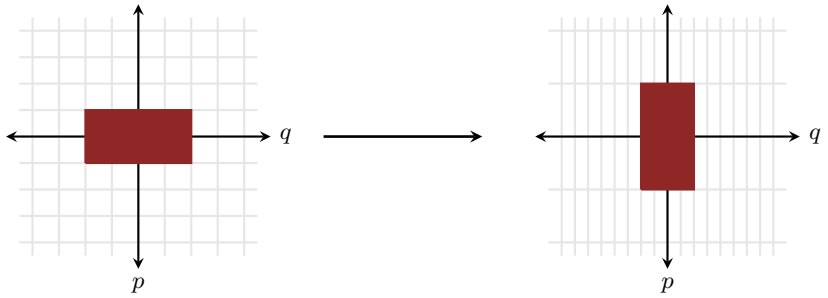

FIG 18. *A defining feature of conservative dynamics is the preservation of volume in position-momentum phase space. For example, although dynamics might compress volumes in position space, the corresponding volume in momentum space expands to compensate and ensure that the total volume is invariant. Such volume-preserving mappings are also known as* shear *transformations.*

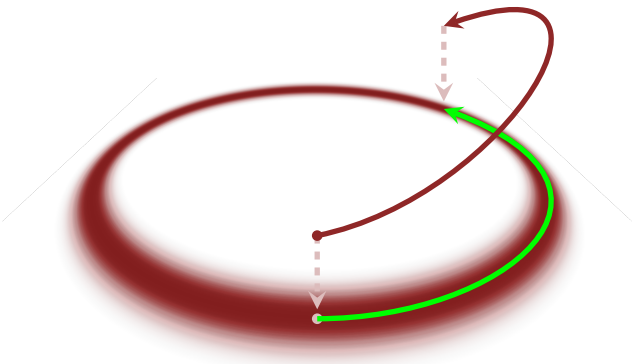

FIG 19. *By constructing a probability distribution on phase space that marginalizes to the target distribution, we ensure that the typical set on phase space projects to the typical set of the target distribution. In particular, if we can construct trajectories that efficiently explore the joint distribution (black) they will project to trajectories that efficiently explore the target distribution (green).*

canonical density $\pi(q, p)$ does not depend on a particular choice of parameterization, and we can write it in terms of an invariant *Hamiltonian* function, $H(q, p)$,

$$\pi(q, p) = e^{-H(q,p)}.$$

Because $H(q, p)$ is independent of the details of any parameterization, it captures the invariant probabilistic structure of the phase space distribution and, most importantly, the geometry of its typical set. Appealing to the physical analogy, the value of the Hamiltonian at any point in phase space is called the *energy* at that point.

Because of the decomposition of the joint density, the Hamiltonian,

$$H(q, p) \equiv -\log \pi(q, p)\,,$$

itself decomposes into two terms,

$$\begin{aligned} H(q, p) &= -\log \pi(p \mid q) - \log \pi(q) \\ &\equiv \quad K(p, q) \quad + \; V(q)\,. \end{aligned}$$

Once again leveraging the physical analogy, the term corresponding to the density over the auxiliary momentum, $K(p, q)$ is called the *kinetic energy*, while the term corresponding to the density of the target distribution, $V(q)$ is known as the *potential energy*. The potential energy is completely determined by the target distribution while the kinetic energy is unconstrained and must be specified by the implementation.

Because the Hamiltonian captures the geometry of the typical set, it should we should be able to use it to generate a vector field oriented with the typical set of the canonical distribution and hence the trajectories that we are after. Indeed, the desired vector field can be generated from a given Hamiltonian with *Hamilton's equations*,

$$\begin{aligned} \frac{\mathrm{d}q}{\mathrm{d}t} &= +\frac{\partial H}{\partial p} = \frac{\partial K}{\partial p} \\ \frac{\mathrm{d}p}{\mathrm{d}t} &= -\frac{\partial H}{\partial q} = -\frac{\partial K}{\partial q} - \frac{\partial V}{\partial q}. \end{aligned}$$

Recognizing $\partial V / \partial q$ as the gradient of the logarithm of the target density, we see that Hamilton's equations fulfill exactly the intuition introduced in Section 3.1. By channeling the gradient through the momentum instead of the target parameters directly, Hamilton's equations twist differential information to align with the typical set of canonical distribution. Following the Hamiltonian vector field for some time, t, generates trajectories, $\phi_t(q, p)$, that rapidly move through phase space while being constrained to the typical set. Projecting these trajectories back down onto the target parameter space finally yields the efficient exploration of the target typical set for which we are searching.

3.3 The Idealized Hamiltonian Markov Transition

In order to utilize these Hamiltonian trajectories to construct an efficient Markov transition, we need a mechanism for introducing momentum to a given point in the target parameter space. Fortunately, this is straightforward if we exploit the probabilistic structure that we have already endowed to the system.

To lift an initial point in parameter space into one on phase space we simply sample from the conditional distribution over the momentum,

$$p \sim \pi(p \mid q) \, .$$

Assuming that the initial point was in the typical set of the target distribution, sampling the momentum directly from the conditional distribution guarantees that the lift will fall into the typical set on phase space.

Once on phase space we can explore the joint typical set by integrating Hamilton's equations for some time,

$$(q, p) \rightarrow \phi_t(q, p) \, .$$

By construction these trajectories coherently push the Markov transition away from the initial point, and neighborhoods that we have already explored, while staying confined to the joint typical set.

Because of the carefully chosen structure of the joint distribution, these trajectories project down to trajectories that explore the target distribution. Consequently, after integrating Hamilton's equations we can return to the target parameter space by simply projecting away the momentum,

$$(q, p) \rightarrow q.$$

Composing these three steps together yields a Hamiltonian Markov transition composed of random trajectories that rapidly explore the target distribution, exactly as desired (Figure 20). Out in the tails of the target distribution, the momentum sampling and projection steps allow the resulting Markov chain to rapidly fall in toward the typical set. Once the chain has reached the typical set, the Hamiltonian trajectories ensure extremely efficiently exploration.

4. EFFICIENT HAMILTONIAN MONTE CARLO

An immediate complication with this foundational construction is that it does not define a unique Markov transition but rather an infinity of them. Every choice of kinetic energy and integration time yields a new Hamiltonian transition that will interact differently with a given target distribution. Unfortunately, these interactions will usually lead to suboptimal performance and we are left with a delicate tuning problem. When these degrees of freedom are well-chosen, the resulting implementation of Hamiltonian Monte Carlo will perform well on even the challenging, high-dimensional problems of applied interest. When they are poorly-chosen, however, the performance can suffer dramatically.

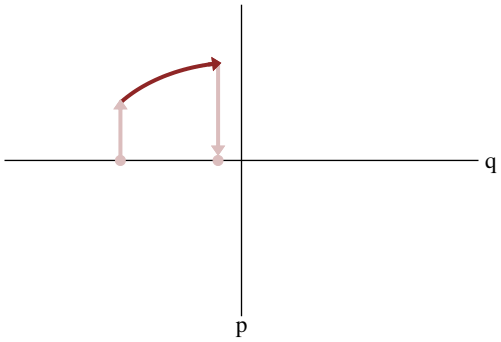

FIG 20. *Every Hamiltonian Markov transition is comprised of a random lift from the target parameter space onto phase space (light red), a deterministic Hamiltonian trajectory through phase space (dark red), and a projection back down to the target parameter space (light red).*

In order to be able to optimize the application of the Hamiltonian Monte Carlo method and ensure robust performance, we need to understand exactly how these degrees of freedom interact with the target distribution. Although this seems like a daunting task, we can facilitate it by exploiting the latent geometry of Hamiltonian Monte Carlo itself. In particular, the analysis is make much easier by considering a different view of phase space.

4.1 The Natural Geometry of Phase Space

One of the characteristic properties of Hamilton's equations is that they conserve the value of the Hamiltonian. In other words, every Hamiltonian trajectory is confined to an energy *level set*,

$$H^{-1}(E) = \{q, p \mid H(q, p) = E\},$$

which, save for some ignorable exceptions, are all $(2D - 1)$-dimensional, compact surfaces in phase space. In fact, once we've removed any singular level sets, the entirety of phase space neatly decomposes, or *foliates* into concentric level sets (Figure 21). Consequently, we can specify any point in phase space by first specifying the energy of the level set it falls on, E, and the position within that level set, θ_E (Figure 21).

Correspondingly the canonical distribution on phase space admits a *microcanonical decomposition*,

$$\pi(q, p) = \pi(\theta_E \mid E)\, \pi(E),$$

across this foliation. The conditional distribution over each level set, $\pi(\theta_E \mid E)$, is called the *microcanonical distribution*, while the distribution across the level sets, $\pi(E)$, is called the *marginal energy distribution*.

Because they are derived from the same geometry, this microcanonical decomposition is particularly well-suited to analyzing the Hamiltonian transition. To see this more clearly, consider a Hamiltonian Markov chain consisting of multiple transitions (Figure 22a). Each

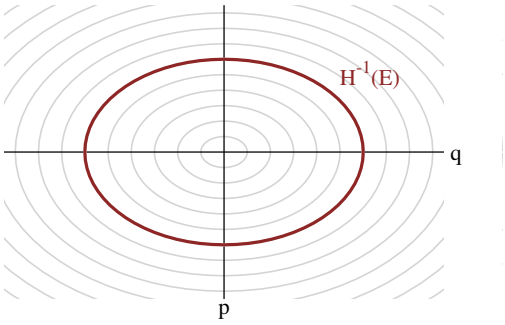

FIG 21. *Phase space naturally decomposes into level sets of the Hamiltonian, $H^{-1}(E)$. Instead of specifying a point in phase space with its position and momentum, we can specify it with an energy, E, and its position on the corresponding level set, $\theta_E \in H^{-1}(E)$.*

Hamiltonian trajectory explores a level set while the intermediate projections and lifts define a random jump between the level sets themselves. Consequently, the entire Hamiltonian Markov chain decouples into two distinct phases: deterministic exploration of individual level sets and a stochastic exploration between the level sets themselves (Figure 22b).

This decoupling makes it particularly convenient to analyze the efficiency of each phase, and hence the efficiency of the overall Hamiltonian Markov transition. For example, the efficacy of the deterministic exploration is determined by how long the Hamiltonian trajectories are integrated and, consequently, how completely they explore the corresponding level sets. The cost of this phase, however, is ultimately proportional to the total integration time. The integration time needed to explore just enough of each level set, and hence the overall efficiency of the deterministic exploration, depends on the geometry of the energy level sets. The more uniform and regular the level sets, the faster the trajectories will explore for a given integration time.

Similarly, the performance of the stochastic exploration is determined by how quickly the random walk can diffuse across the energies typical to the marginal energy distribution. Writing $\pi(E \mid q)$ as the transition distribution of energies induced by a momentum resampling at a given position, q, the diffusion speed depends on how heavy-tailed the marginal energy distribution is relative to $\pi(E \mid q)$. For example, if this energy transition distribution is narrow relative to the marginal energy distribution (Figure 23a), then the random walk will proceed very slowly, taking many costly transitions to completely explore the target distribution. If the energy transition distribution is similar to the marginal energy distribution (Figure 23b), however, then we will generate nearly-independent samples from the marginal energy distribution at every transition, rapidly surveying the relevant energies with maximal efficiency.

By analyzing how these algorithmic degrees of freedom in the Hamiltonian Markov transition interact with the target distribution to determine the microcanonical geometry,

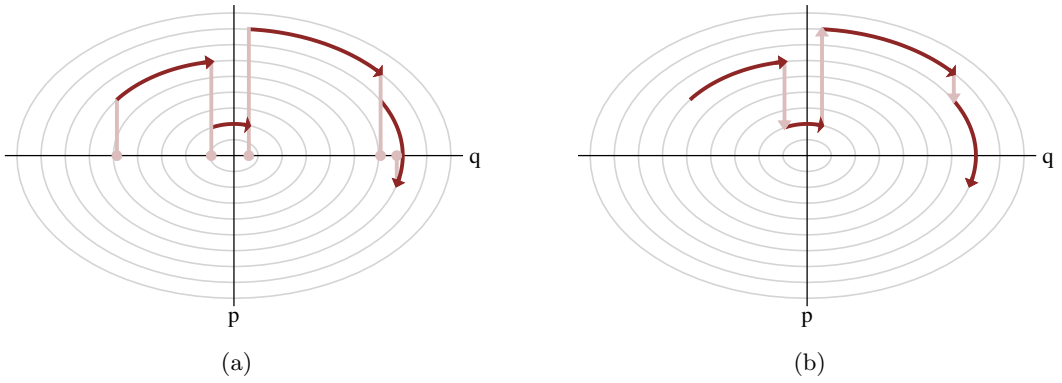

FIG 22. *(a) Each Hamiltonian Markov transition lifts the initial state onto a random level set of the Hamiltonian, which can then be explored with a Hamiltonian trajectory before projecting back down to the target parameter space. (b) If we consider the projection and random lift steps as a single momentum resampling step, then the Hamiltonian Markov chain alternates between deterministic trajectories along these level sets (dark red) and a random walk across the level sets (light red).*

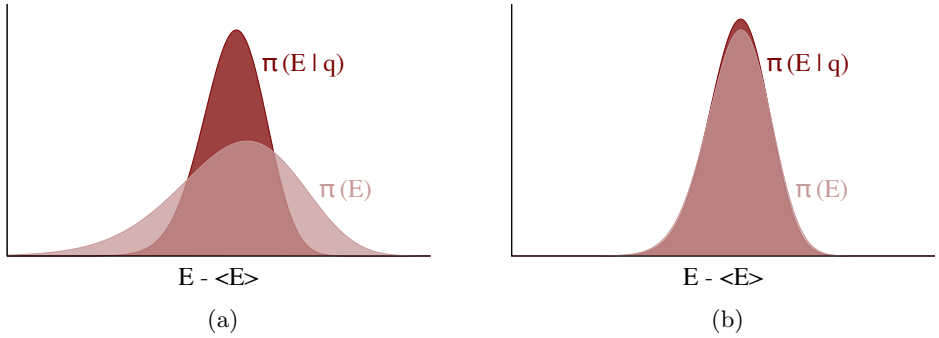

FIG 23. *The momentum resampling in a Hamiltonian Markov transition randomly changes the energy, inducing a random walk between level sets. (a) When the energy transition distribution, $\pi(E \mid q)$ is narrow relative to the marginal energy distribution, $\pi(E)$, this random walk will explore the marginal energy distribution only very slowly, requiring many expensive transitions to survey all of the relevant energies. (b) On the other hand, when the two distributions are well-matched the random walk will explore the marginal energy distribution extremely efficiently.*

we can determine how they affect the performance of the resulting Hamiltonian Markov chain. In particular, we can construct criteria that identify the optimal choices of these degrees of freedom, which then motivate the effective tuning of the method, even for the complex target distributions encountered in practice.

4.2 Optimizing the Choice of Kinetic Energy

The first substantial degree of freedom in the Hamiltonian Monte Carlo method that we can tune is the choice of the conditional probability distribution over the momentum or, equivalently, the choice of a kinetic energy function. Along with the target distribution, this choice completes the probabilistic structure on phase space which then determines the geometry of the microcanonical decomposition. Consequently, the ideal kinetic energy will interact with the target distribution to ensure that the energy level sets are as uniform as possible while the energy transition distribution matches the marginal energy distribution as well as possible.

Unfortunately, there is an infinity of possible kinetic energies and it would be impossible to search through them all to find an optimal choice for any given target distribution. It is much more practical to search through a restricted family of kinetic energies, especially if that family is built from the structure of the problem itself.

4.2.1 Euclidean-Gaussian Kinetic Energies For example, in many problems the sample space is endowed with a Euclidean metric, g, that allows us to measure, amongst other quantities, the distance between any two points. In a given parameterization, g is represented with a $D \times D$ matrix from which we can compute distances as

$$\Delta(q, q') = (q - q')^T \cdot g \cdot (q - q'),$$

Moreover, we can construct an entire family of modified Euclidean metrics, M, by scaling and then rotating this natural metric,

$$M = R \cdot S \cdot g \cdot S^T \cdot R^T,$$

where S is a diagonal scaling matrix and R is an orthogonal rotation matrix.

Any such Euclidean structure on the target parameter space immediately induces an inverse structure on the momentum space, allowing us to measure distances between momenta,

$$\Delta(p, p') = (p - p')^T \cdot M^{-1} \cdot (p - p').$$

Finally, distances in momentum space allow us to construct many common probability distributions over the momentum, such as a Gaussian distribution centered at 0,

$$\pi(p \mid q) = \mathcal{N}(p \mid 0, M)\,.$$

This particular choice defines a *Euclidean-Gaussian* kinetic energy,

$$K(q, p) = \frac{1}{2} p^T \cdot M^{-1} \cdot p + \log |M| + \text{const.}$$

In the physical perspective the Euclidean metric is known as the *mass matrix*, a term that has consequently become common in the Hamiltonian Monte Carlo literature.

Because the Euclidean structure over the momentum is dual to the Euclidean structure over the parameters, its interactions with the target distribution are straightforward to derive. Applying the transformation $p' = \sqrt{M^{-1}} p$ simplifies the kinetic energy, but remember that we have to apply the *opposite* transformation to the parameters, $q' = \sqrt{M} q$, to preserve the Hamiltonian geometry. Consequently, a choice of M^{-1} effectively rotates and then rescales the target parameter space, potentially correlating or de-correlating the target distribution and correspondingly warping the energy level sets.

In particular, as the inverse Euclidean metric more closely resembles the covariance of the target distribution it de-correlates the target distribution, resulting in energy level sets that are more and more uniform and hence easier to explore. We can then readily optimize over the family of Euclidean-Gaussian kinetic energies by setting the inverse Euclidean metric to the target covariances,

$$M^{-1} = \mathbb{E}_{\pi}[(q - \mu)\,(q - \mu)^{T}].$$

In practice we can compute an empirical estimate of the target covariance using the Markov chain itself in an extended warm-up phase. After first converging to the typical set we run the Markov chain using a default Euclidean metric for a short window to build up an initial estimate of the target covariance, then update the metric to this estimate before running the now better-optimized chain to build up an improved estimate. A few iterations of this adaptation will typical yield an accurate estimate of the target covariance and hence a near-optimal metric.

4.2.2 Riemannian-Gaussian Kinetic Energies Unless the target distribution is exactly Gaussian, however, no global rotation and rescaling will yield completely uniform level sets; locally the level sets can still manifest strong curvature that slows the exploration of the Hamiltonian trajectories. To improve further we need to introduce a *Riemannian* metric which, unlike the Euclidean metric, varies as we move through parameter space. A Riemannian structure allows us to construct a Gaussian distribution over the momentum whose covariance depends on our current position in parameter space,

$$\pi(p \mid q) = \mathcal{N}(p \mid 0, \Sigma(q))\,,$$

which then defines a *Riemannian-Gaussian* kinetic energy,

$$K(q, p) = \frac{1}{2} p^{T} \cdot \Sigma^{-1}(q) \cdot p + \frac{1}{2} \log |\Sigma(q)| + \text{const.}$$

The resulting implementation of Hamiltonian Monte Carlo is known as *Riemannian Hamiltonian Monte Carlo* (Girolami and Calderhead, 2011).

The variation of the inverse Riemannian metric allows it to make local corrections to the target distribution that vary depending on where we are in parameter space. If the metric

resembles the Hessian of the target distribution then these local corrections will rectify the spatially-varying correlations of the target distribution, ensuring extremely uniform level sets and efficient exploration. Technical care, however, must be taken when trying to mimic the Hessian to ensure that the inverse Riemannian metric, and hence the entire kinetic energy is well-behaved; the SoftAbs metric (Betancourt, 2013a) accomplishes this with a heuristic regularization that works well in practice, although formalizing this procedure is an active topic of research (Holmes, Rubinstein-Salzedo and Seiler, 2014).

An additional benefit of the Riemannian-Gaussian kinetic energy is that the variation of the log determinant, $\frac{1}{2} \log |\Sigma(q)|$, modifies the marginal energy distribution. If the metric is well-chosen then this modification can bring the marginal energy distribution closer to the energy transition distribution, significantly improving the performance of the Hamiltonian transition when targeting complex distributions (Betancourt and Girolami, 2015).

4.2.3 Non-Gaussian Kinetic Energies In theory we are not limited to Gaussian distributions over the momentum – a Euclidean or Riemannian structure allows us to construct any distribution with quadratic sufficient statistics. In particular, why should we not consider momentum distributions with particularly heavy or light tails? Although there is not much supporting theory, empirically non-Gaussian kinetic energies tend to perform poorly, especially in high-dimensional problems. Some intuition for the superiority of Gaussian kinetic energies may come from considering the asymptotics of the marginal energy distribution. As we target higher and higher dimensional models, the marginal energy distribution becomes a convolution of more and more parameters and, under relatively weak conditions, it tends to follow a central limit theorem. When the marginal energy distribution converges towards a Gaussian, only a Gaussian distribution over the momentum will yield the optimal energy transition.

4.3 Optimizing the Choice of Integration Time

The choice of a kinetic energy completely specifies the microcanonical geometry and, consequently, the shape of the energy level sets. How effectively each Hamiltonian trajectory explores those level sets is then determined entirely by the choice of integration times across phase space, $T(q, p)$. Intuitively, if we integrate for only a short time then we don't take full advantage of the coherent exploration of the Hamiltonian trajectories and we will expect performance to suffer. On the other hand, because the level sets are topologically compact in well-behaved problems, trajectories will eventually return to previously explored neighborhoods and integrating too long can suffer from diminishing returns.

This intuition is formalized in the notion of *dynamic ergodicity* (Betancourt, 2016a). Here we consider the *orbit*, ϕ, of a trajectory, consisting of all points that the trajectory will reach as the integration time is increased to infinity. The orbit might encompass the entire level set or it could be limited to a just subset of the level set, but in either case any trajectory will explore the microcanonical distribution restricted to its orbit. Dynamic ergodicity guarantees that a uniform sample from a trajectory will more closely resemble a sample from this restricted microcanonical distribution as the integration time is increased

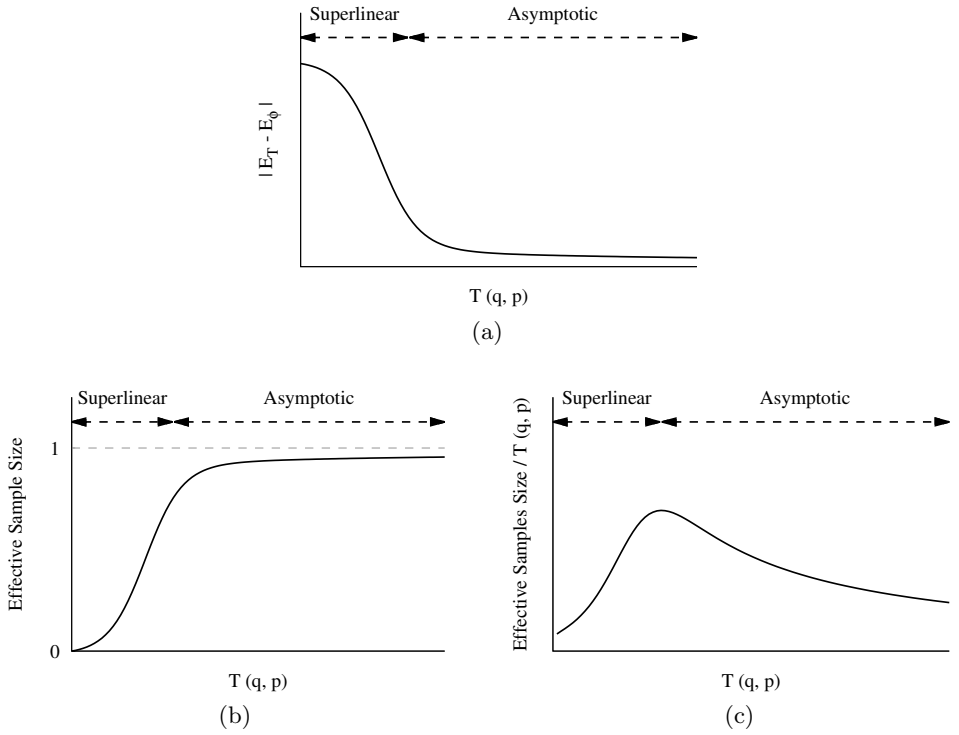

FIG 24. *(a) Temporal averages along a Hamiltonian trajectory, $\mathbb{E}_T$, converge to the corresponding spatial expectation over its orbit, $\mathbb{E}_\phi$, as the integration time, T, increases. (b) Correspondingly, a uniform sample from the trajectory converges to a sample from the microcanonical distribution restricted to the trajectory's orbit, here represented by the effective sample size. Typically this convergence is initially rapid and superlinear before settling into an asymptotic regime where the convergence continues only with the square of the integration time. (c) Because the cost of generating each trajectory scales with the integration time, those integration times that identify the transition between these two regimes will yield optimal performance.*

and the trajectory grows. In other words, as the integration time grows the temporal expectation over the trajectory converges to the spatial expectation over its orbit.

The performance of the Hamiltonian transition, however, depends on the *rate* at which these expectations converge. Given typical regularity conditions, the temporal expectation will initially converges toward the spatial expectation quite rapidly (Figure 24a, b), consistent with our intuition that coherent exploration is extremely effective. Eventually, however, that convergence slows, and we enter an asymptotic regime where any benefit of exploration comes at an ever increasing cost. The optimal integration time straddles these two regimes, exploiting the coherent exploration early on but not wasting computation on the diminishing returns of long integration times (Figure 24c).

This optimization criterion also has a helpful geometric interpretation. The superlinear regime corresponds to the first sojourn around the orbit of the trajectory, where every new

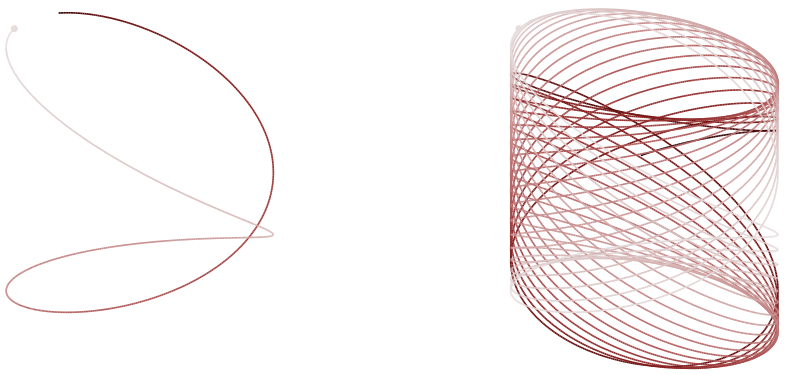

(a) (b)

FIG 25. *(a) Because a Hamiltonian trajectory's first sojourn through its orbit continuously encounters new, un-surveyed neighborhoods, the corresponding exploration is extremely efficient. (b) Longer trajectories return to these neighborhoods, refining this initial exploration and yielding better, but much slower, convergence.*

step forwards is new and informative (Figure 25a). Eventually, however, the trajectory returns to neighborhoods it has already explored and enters into the asymptotic regime (Figure 25b). This additional exploration refines the exploration of the orbit, improving the accuracy of the temporal expectation only very slowly.

In general, this optimal integration time will vary strongly depending on which trajectory we are considering: no single integration time will perform well everywhere. We can make this explicit in one dimension where the optimal integration times can be identified analytically. For example, for the family of target densities

$$\pi_\beta(q) \propto e^{-|q|^\beta},$$

with the Euclidean-Gaussian kinetic energy

$$\pi(p \mid q) = \mathcal{N}(0, 1)\,,$$

the optimal integration time scales with the energy of the level set containing the trajectory,

$$T_{\text{optimal}}(q, p) \propto (H(q, p))^{\frac{2-\beta}{2\beta}}\,.$$

In particular, when the target distribution is heavy-tailed, $\beta < 2$, the optimal integration time will quickly grow as we move from trajectories exploring the bulk to trajectories exploring the tails (Figure 26). Consequently, the exploration generated by trajectories

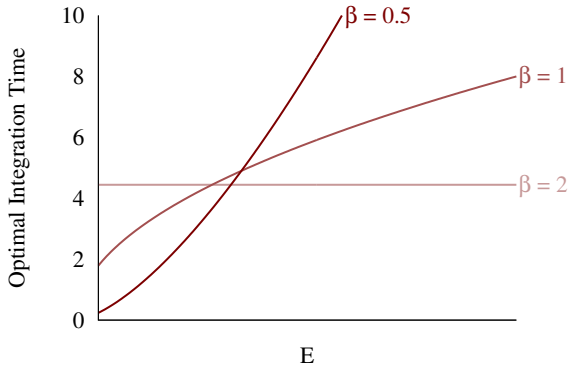

FIG 26. *The spatial variation of optimal integration times is evident in a one-dimensional example where the optimal integration times can be calculated analytically and are found to scale with the energy of the initial point in phase space. Only for a Gaussian target distribution, $\beta = 2$, are the optimal integration times constant for all energies. The optimal integration time for heavy-tailed target distributions, $\beta < 2$, grows larger as we move deeper into the tails with higher energies. A given static integration time might suffice for low energies, but it will yield trajectories that are much too short for any effective exploration of the higher energy level sets.*

with any *static* integration time will decay and the Hamiltonian Markov chain will slow to a crawl.

Hence if we want to fully exploit these Hamiltonian trajectories then we need to identify the optimal integration time *dynamically*, as we generate the trajectories themselves. How exactly do we identify when a trajectory has reached its optimal length? One heuristic is the No-U-Turn termination criterion (Hoffman and Gelman, 2014; Betancourt, 2013b) which, like the kinetic energies discussed in Section 4.2, utilizes a Euclidean or Riemannian structure on the target parameter space. The explicit form of the No-U-Turn termination criterion is introduced in Appendix A.4.2.

In some simple cases the near-optimality of the No-U-Turn criterion can be shown rigorously, but it has proven a empirical success on an incredibly diverse set of target distributions encountered in applied problems. More recently proposed possibilities are exhaustive termination criteria (Betancourt, 2016a) which utilize the microcanonical geometry itself to identify the optimal stopping time. Exhaustive termination criteria can be more robust than the No-U-Turn termination criterion, but they require careful tuning which is an open topic of research.

5. IMPLEMENTING HAMILTONIAN MONTE CARLO IN PRACTICE

With careful tuning, the Hamiltonian Monte Carlo method defines a powerful Markov transition capable of performing well over a large class of target distributions, at least in theory. Unfortunately, there are almost no Hamiltonian transitions that are immediately applicable *in practice*.

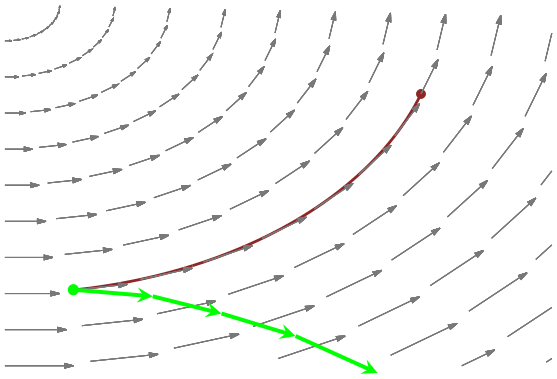

FIG 27. *The approximate solutions of most numerical integrators tend to drift away from the exact solutions. As the system is integrated longer and longer, errors add coherently and push the numerical trajectory away from the exact trajectory.*

The main obstruction to implementing the Hamiltonian Monte Carlo method is generating the Hamiltonian trajectories themselves. Aside from a few trivial examples, we cannot solve Hamilton's equations exactly and any implementation must instead solve them numerically. Numerical inaccuracies, however, can quickly compromise the utility of even the most well-tuned Hamiltonian transition. Formally, integrating along the vector field defined by Hamilton's equations is equivalent to solving a system of ordinary differential equations on phase space. The more accurately we can numerically solve this system, the more effective our implementation will be.

While there is an abundance of ordinary differential equations solvers, or numerical integrators, available in popular computational libraries, most of those solvers suffer from an unfortunate *drift*. As we numerically solve longer and longer trajectories the error in the solvers adds coherently, pushing the approximate trajectory away from the true trajectory and the typical set that we want to explore (Figure 27). Because the magnitude of this drift rapidly increases with the dimension of phase space, the utility of these generic numerical integrators is limited to approximating only short Hamiltonian trajectories that inefficiently explore the energy level sets.

Fortunately, we can use the geometry of phase space itself to construct an extremely powerful family of numerical solvers, known as *symplectic integrators* (Leimkuhler and Reich, 2004; Hairer, Lubich and Wanner, 2006), that are robust to phenomena like drift and enable high-performance implementations of the Hamiltonian Monte Carlo method. In this section I will present the practical properties of symplectic integrators and how we can correct for the small errors that they introduce. We will conclude with a discussion of how to choose the best symplectic integrator for a given problem.

This section will follow the conceptual presentation of the review, but given the importance of the material a more thorough discussion of the technical details is available in

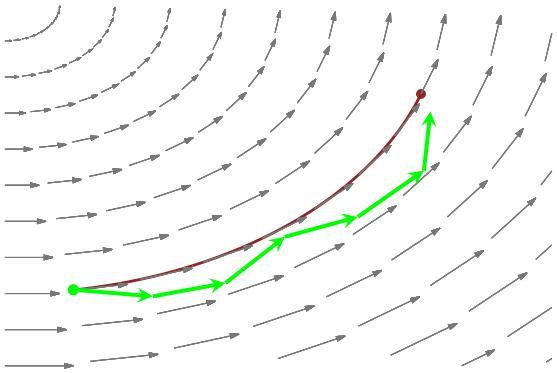

FIG 28. *Symplectic integrators generate numerical trajectories that are incompressible like the exact Hamiltonian trajectory they approximate. Consequently their approximation error cannot add up coherently to pull the numerical trajectories away from the exact trajectories. Instead the numerical trajectories oscillate around the exact level set, even as we integrate for longer and longer times.*

Appendix A.

5.1 Symplectic Integrators

Symplectic integrators are powerful because the numerical trajectories they generate exactly preserve phase space volume, just like the Hamiltonian trajectories they are approximating. This incompressibility limits how much the error in the numerical trajectory can deviate from the energy of the exact trajectory. Consequently, the numerical trajectories cannot drift away from the exact energy level set, instead oscillating near it even for long integration times (Figure 28).

Conveniently for implementations, symplectic integrators are also straightforward to implement in practice. For example, if the probabilistic distribution of the momentum is chosen to be independent of position, as with the Euclidean-Gaussian kinetic energy, then we can employ the deceptively simple *leapfrog integrator*. Given a time discretization, or step size, ϵ, the leapfrog integrator simulates the exact trajectory as

$q_0 \leftarrow q, p_0 \leftarrow p$
for $0 \leq n < \llcorner T / \epsilon \lrcorner$ **do**
  $p_{n+\frac{1}{2}} \leftarrow p_n - \frac{\epsilon}{2} \frac{\partial V}{\partial q}(q_n)$
  $q_{n+1} \leftarrow q_n + \epsilon \, p_{n+\frac{1}{2}}$
  $p_{n+1} \leftarrow p_{n+\frac{1}{2}} - \frac{\epsilon}{2} \frac{\partial V}{\partial q}(q_{n+1})$
end for.

This simple but precise interleaving of discrete momentum and position updates ensures exact volume preservation on phase space, and hence the accurate numerical trajectories

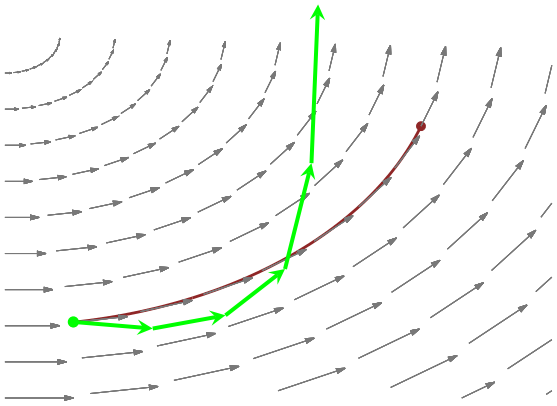

FIG 29. *When the exact trajectories lie on energy level sets with regions of high curvature, the numerical trajectories generated by symplectic integrators can diverge, rapidly flying off towards the boundaries of phase space. Unlike the slower drift of generic numerical integrators, these divergences, and hence the failure of the symplectic integrator to provide an accurate solution, are straightforward to identify in practice.*

we need to realize the potential of a Hamiltonian transition.

There is, however, one important exception to performance of symplectic integrators. Long time accuracy can be compromised when the exact energy level sets feature neighborhoods of high curvature that the finite time discretization is not able to resolve. These neighborhoods induce a *divergence* that almost immediately propels the numerical trajectory towards infinite energies (Figure 29). This distinctive behavior proves beneficial in practice, however, because it makes the failures of a symplectic integrator straightforward to identify and hence diagnose.

Employing symplectic integrators provides the opportunity to translate the theoretical performance of the Hamiltonian Monte Carlo method into a practical implementation. There remain, however, two obstructions to realizing this translation. First, even though symplectic integrators are highly accurate, the small errors they do introduce will bias the resulting Hamiltonian transitions without an exact correction. Second, we have to be able to select a symplectic integrator well-suited to a given target distribution.

5.2 Correcting for Symplectic Integrator Error

One particularly natural strategy for correcting the bias introduced by the error in a symplectic integrator is to treat the Hamiltonian transition as the proposal for a Metropolis-Hastings scheme on phase space. If we can construct the acceptance probability analytically then this correction will yield an exact sample from the canonical distribution on phase space which then projects to an exact sample from our target distribution. In order to construct that acceptance probability, however, we have to carefully augment the Hamiltonian transition.

For example, consider a simple scheme where we integrate the initial state, (q_0, p_0), for-

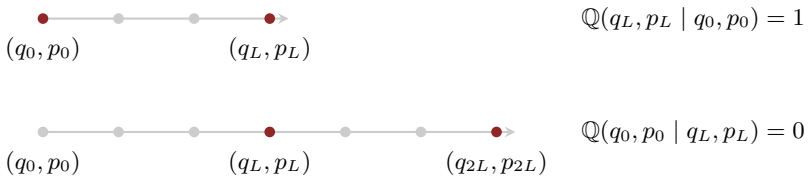

FIG 30. *Because Hamiltonian trajectories, and their numerical approximations, are deterministic and non-reversible, Metropolis-Hastings proposals are always rejected. In particular, we have positive proposal probabilities going forwards in time but vanishing proposal probabilities going backwards in time which renders the Metropolis-Hastings acceptance probability identically zero.*

ward for some static time, or equivalently L symplectic integrator steps, and then propose the last state of the numerical trajectory, (q_L, p_L),

$$\mathbb{Q}(q', p' \mid q_0, p_0) = \delta(q' - q_L)\, \delta(p' - p_L).$$

Because we can propose only states going forwards and not backwards, (Figure 30), the ratio of proposal densities, and hence the Metropolis-Hastings acceptance probability, always vanishes,

$$\frac{\mathbb{Q}(q_0, p_0 \mid q_L, p_L)}{\mathbb{Q}(q_L, p_L \mid q_0, p_0)} = \frac{0}{1}.$$

If we modify the Hamiltonian transition to be *reversible*, however, then the ratio of proposal densities becomes non-zero and we achieve a useful correction scheme. The simplest way of achieving a reversible proposal is to augment the the numerical integration with a negation step that flips the sign of momentum,

$$(q, p) \to (q, -p)\,.$$

This yields the reversible proposal (Figure 31)

$$\mathbb{Q}(q', p' \mid q_0, p_0) = \delta(q' - q_L)\, \delta(p' + p_L),$$

with the corresponding Metropolis-Hastings acceptance probability

$$\begin{aligned}
a(q_L, -p_L \mid q_0, p_0) &= \min\left(1, \frac{\mathbb{Q}(q_0, p_0 \mid q_L, -p_L)\, \pi(q_L, -p_L)}{\mathbb{Q}(q_L, -p_L \mid q_0, p_0)\, \pi(q_0, p_0)}\right) \\
&= \min\left(1, \frac{\delta(q_L - q_L)\, \delta(-p_L + p_L)\, \pi(q_L, -p_L)}{\delta(q_0 - q_0)\, \delta(p_0 - p_0)\, \pi(q_0, p_0)}\right) \\
&= \min\left(1, \frac{\pi(q_L, -p_L)}{\pi(q_0, p_0)}\right) \\
&= \min\left(1, \frac{\exp\left(-H(q_L, -p_L)\right)}{\exp\left(-H(q_0, p_0)\right)}\right) \\
&= \min(1, \exp\left(-H(q_L, -p_L) + H(q_0, p_0)\right))\,,
\end{aligned}$$

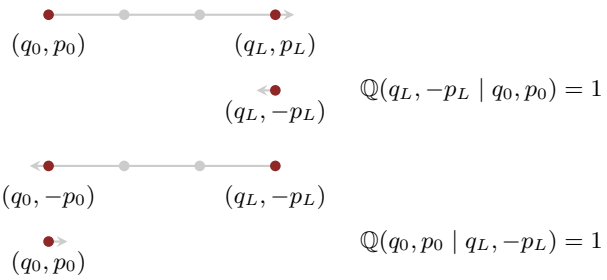

FIG 31. *Augmenting the numerical trajectory with a momentum flip defines a reversible Metropolis-Hastings proposal for which the forwards and backwards proposal probabilities are both well-behaved and we recover a valid correction scheme.*

Because we can always evaluate the Hamiltonian, we can immediately construct the acceptance probability and then correct for the bias induced by the symplectic integrator error. Moreover, because symplectic integrators oscillate near the exact energy level set this acceptance probability will deteriorate only negligibly as we consider target distributions of higher and higher dimensions.

Our analysis of optimal integration times in Section 4.3, however, motivated taking not the last state from a Hamiltonian trajectory but rather sampling points uniformly from the entire trajectory to best approximate a sample from the microcanonical distribution. We can modify our Metropolis-Hastings approach towards this end by proposing not just the final point but all points in the numerical trajectory,

$$\mathbb{Q}(q', p' \mid q_0, p_0) = \frac{1}{L} \sum_{l=0}^{L} \delta(q' - q_l) \, \delta(p' + p_l).$$

This generalized proposal is still reversible and the acceptance probability similarly reduces to

$$a(q_l, -p_l \mid q_0, p_0) = \min(1, \exp\left(-H(q_l, -p_l) + H(q_0, p_0)\right)),$$

for $0 \leq l \leq L$ and vanishes otherwise.

Unfortunately, this generalized proposal can suffer from sub-optimal performance because it proposes states independent of their acceptance probability. In particular, we can propose a state with large error and be forced to reject the proposal even though there are might be other states in the numerical trajectory with much smaller errors and correspondingly higher acceptance probabilities. To achieve optimal performance we have to *average* the proposals to all states in the trajectory into a single, efficient proposal.

There are numerous schemes for achieving such an average, and they all require generating numerical trajectories by integrating the initial state not only forwards in time but also backwards. Once we start integrating in both directions it becomes easier to reason about the Hamiltonian Markov transition as a two-stage process. First we uniformly sample a

trajectory, $\mathfrak{t}$, from all numerical trajectories of length L that contain the initial point, and then we sample a point from that trajectory with the probabilities

$$\pi(q, p) = \frac{e^{-H(q,p)}}{\sum_{(q',p') \in \mathfrak{t}} e^{-H(q',p')}}.$$

Detailed proofs demonstrating the validity of this scheme, and its extension to dynamic trajectory lengths, can be found in Appendix A.

5.3 Optimal Choice of Symplectic Integrator

Now that we know how to implement the Hamiltonian Monte Carlo method with symplectic integrators, we are left with the choice of the exact configuration of the symplectic integrator itself. These configurations are characterized with a choice of step size, ϵ, and an order, K, that quantifies how many gradient evaluations are used in each discrete integrator step.

In general there is a delicate balance between configurations that are more accurate but more expensive, and those that are less accurate but cheaper. For example, regardless of the exact order of the integrator, the step size will control the number of integrator steps, $L = T/\epsilon$, and hence the overall cost of each Hamiltonian transition. Smaller step sizes yield more accurate numerical trajectories and better exploration, but at the expense of many more integrator steps. Similarly, the higher the order of the integrator the more accurate, but also more expensive, it will be.

Fortunately, this intuition can be formalized and quantified by exploiting the geometry inherent to symplectic integrators. In particular, the volume preservation of symplectic integrators guarantees not only that they well-approximate trajectories generated by the exact Hamiltonian, but also that they exactly solve trajectories generated by some *modified Hamiltonian* or *shadow Hamiltonian*. This implies that numerical trajectories will be confined to energy level sets of this modified Hamiltonian, and we can quantify the performance of the integrator by studying the differences between the exact and modified level sets (Figure 32a). For example, divergences occur when the modified level sets become non-compact and extend out to the boundaries of phase space (Figure 32b).

When the modified level sets are well-behaved and we do not encounter any divergences, we can quantify the performance of the symplectic integrator by comparing the shapes of the exact and modified level sets. For the simple implementation of Hamiltonian Monte Carlo where we integrate for a static time, T, flip the momentum, and apply a Metropolis-Hastings correction to the final state, this comparison bounds the relationship between the cost of the algorithm and the average Metropolis-Hastings acceptance probability, which itself depends on the step size (Betancourt, Byrne and Girolami, 2014) (Figure 33). These bounds provide the basis for an automated tuning algorithm that adapts the step size during an extended warm-up to achieve an average Metropolis acceptance probability between 0.6 and 0.8, similar to the adaptation of the Euclidean metric discussed in Section

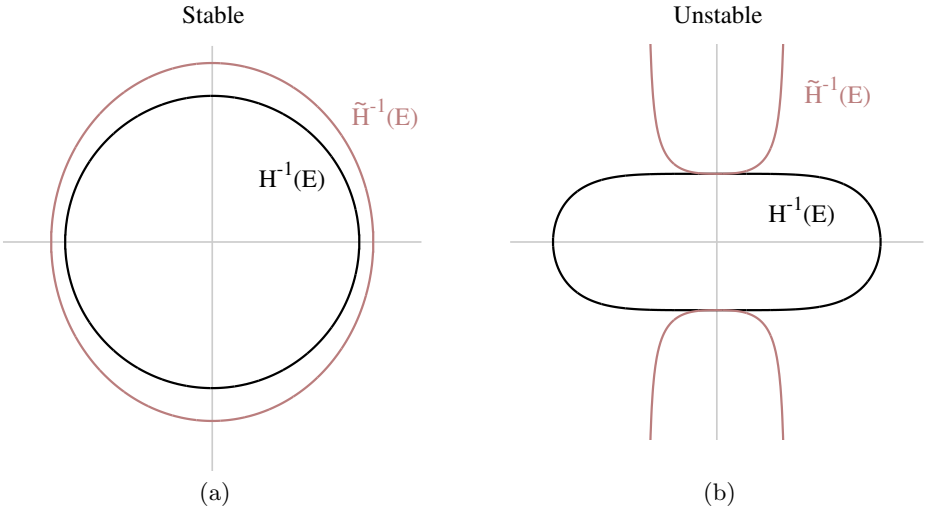

FIG 32. *Symplectic integrators generate exact trajectories from a modified Hamiltonian, $\widetilde{H}$ that resembles the exact Hamiltonian, H, and we can quantify the accuracy of a symplectic integrator by comparing the corresponding energy level sets. (a) When the level sets of the modified Hamiltonian share the same topology as the level sets of the exact Hamiltonian, the numerical trajectories will be stable and highly accurate. (b) When the modified level sets have a different topology, however, the numerical trajectories will become unstable and diverge.*

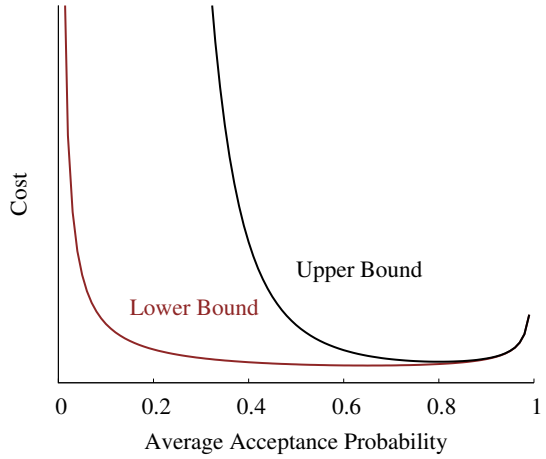

FIG 33. *By comparing the geometry of the modified level sets induced by a symplectic integrator with the exact level sets we can compute bounds between the computational cost of a Hamiltonian transition and the average Metropolis acceptance probability, at least for simple implementations of the Hamiltonian Monte Carlo method. These bounds then inform adaptation procedures that tune the integrator step size to achieve an average acceptance probability that yields minimal cost.*

4.2.1. Although much of this analysis carries over to more sophisticated implementations of Hamiltonian Monte Carlo, more work is needed to formalize the corresponding results.

Finally we are left to consider the order of the symplectic integrator. Most discussions of Hamiltonian Monte Carlo consider only the first-order leapfrog integrator due to its simplicity and empirical success. Recent work, however, has suggested that higher-order integrators may prove more effective, especially in higher-dimensional problems (Blanes, Casas and Sanz-Serna, 2014; Fernández-Pendás, Akhmatskaya and Sanz-Serna, 2015). One serious complication introduced by higher-order integrators are additional degrees of freedom that can significantly affect performance – poor choices of these integrator parameters can completely neutralize any gains over the leapfrog integrator. Understanding how these additional integrator degrees of freedom interact with a given problem, and then developing automated adaptation procedures, is an important next step to the inclusion of higher-order methods.

6. THE ROBUSTNESS OF HAMILTONIAN MONTE CARLO

Up to this point we have been focused on why Hamiltonian trajectories rapidly explore a given target distribution and then how we can configure Hamiltonian Markov transitions to maximize the efficiency of this exploration. We have not yet, however, addressed the critical question of how robust that exploration will be – even the fastest algorithm is worthless if it does not quantify all of the typical set. As discussed in Section 2.3, the formal question we have to consider is for what target distributions will an implementation

of Hamiltonian Monte Carlo be geometrically ergodic and yield well-behaved, unbiased Markov chain Monte Carlo estimators?

Because this question is so general, theoretical analysis is extremely difficult. Preliminary results, however, show that even simple implementations of the Hamiltonian Monte Carlo method are geometrically ergodic over a large class of target distributions (Livingstone et al., 2016). In particular, this class is significantly larger than the class for non-gradient based algorithms like Random Walk Metropolis, consistent with the intuition that gradients are critical to robust Markov chain Monte Carlo in high-dimensional problems.

Perhaps more importantly, this theoretical analysis identifies the pathological behaviors of a target distribution that obstruct geometric ergodicity. Moreover, the work demonstrates that these pathologies manifest in precise empirical behaviors that immediately motivate practical diagnostics unique to Hamiltonian Monte Carlo.

6.1 Diagnosing Poorly-Chosen Kinetic Energies

For example, one pathological behavior that frustrates geometric ergodicity is heavy tails in the target distribution. Heavy tails cause the typical set to push deep into the extremes of parameter space, requiring that any successful Markov chain make prolonged sojourns to the tails and back lest the chain miss significant regions of the typical set.

The progressively long trajectories enabled by dynamic integration time implementations facilitate these sojourns in Hamiltonian Markov chains, but sometimes even exponentially growing integration times can be insufficient. In particular, if the kinetic energy is poorly-chosen then the marginal energy distribution can become heavy-tailed itself in which case the stochastic exploration between level sets will become so slow that after any finite number of transitions the exploration of the Markov chain will be incomplete.

Fortunately, such ill-suited kinetic energies are easy to identify by visualizing the marginal energy density and energy transition density using the Markov chain itself (Betancourt, 2016b) (Figure 34). This visualization quickly identifies when the momentum resampling will inefficiently explore the energy level sets, especially when aggregating multiple chains initialized from diffuse starting points. We can also formalize the mismatch between these two distributions using the Bayesian fraction of missing information,

$$\text{E-BFMI} \equiv \frac{\mathbb{E}_{\pi}\left[\text{Var}_{\pi_{E|q}}[E \mid q]\right]}{\text{Var}_{\pi_E}[E]} \approx \widehat{\text{E-BFMI}} \equiv \frac{\sum_{n=1}^{N} \left(E_n - E_{n-1}\right)^2}{\sum_{n=0}^{N} \left(E_n - \bar{E}\right)^2}.$$

Empirically, values of this energy Bayesian fraction of missing information below 0.3 have proven problematic, although more theoretical work is needed to formalize any exact threshold.

6.2 Diagnosing Regions of High Curvature

Another common obstruction to geometric ergodicity is neighborhoods in parameter space where the target distribution exhibits large curvature. As we saw in Section 2.3,

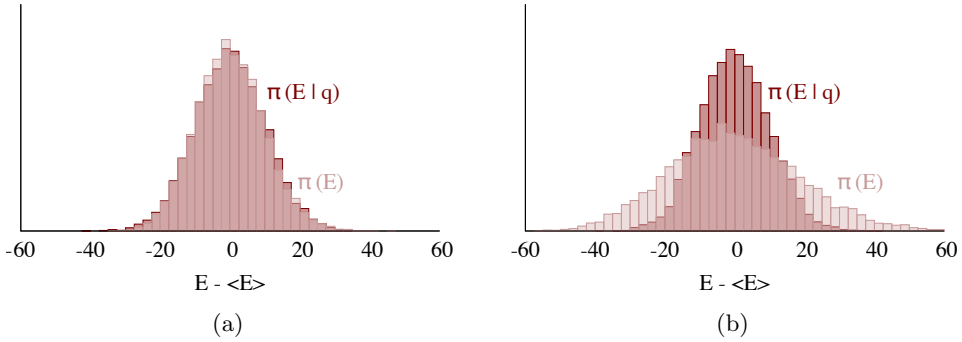

FIG 34. *The energies explored by a Hamiltonian Markov chain can be used to visualize both the energy transition density, $\pi(E \mid q)$, and the marginal energy distribution, $\pi(E)$. (a) When these distributions are well-matched the Hamiltonian Markov chain should perform robustly, (b) but if the energy transitions density is significantly narrower than the marginal energy distribution then the chain may not be able to completely explore the tails of the target distribution.*

most Markov transitions are not able to resolve these narrow neighborhoods, resulting in incomplete exploration and biased Markov chain Monte Carlo estimators. Hamiltonian Markov transitions are no exception. Because such neighborhoods are characteristic of many important models, in particular hierarchical models (Betancourt and Girolami, 2015), these pathologies cannot be ignored in applied practice.

Conveniently, these neighborhoods of high curvature also prove pathological to symplectic integrators, which become unstable and diverge once they enter (Figure 35). Importantly, this means that divergent numerical trajectories are extremely sensitive identifiers of these pathological neighborhoods and hence provide a powerful and immediate diagnostic.

In particular, any divergent transitions encountered in a Hamiltonian Markov chain should prompt suspicion of the validity of any Markov chain Monte Carlo estimators. When the pathologies are sufficiently mild, the divergences can be eliminated, and the validity of the estimators restored, by decreasing the step size of the symplectic integrator. Often, however, the pathologies are too severe and the divergences will persist regardless of the how much the step size is decreased, indicating significant bias in the resulting estimators. In these cases the target distribution itself needs to be regularized, for example with stronger priors or an alternative representation. A prevalent example of the latter is alternating between centered and non-centered parameterizations in latent Gaussian models (Betancourt and Girolami, 2015).

6.3 Limitations of Diagnostics

Although these two diagnostics are powerful means of identifying many pathological target distributions, they are only necessary and not sufficient conditions for the validity of the Markov chain Monte Carlo estimators. Without an explicit theoretical analysis, there

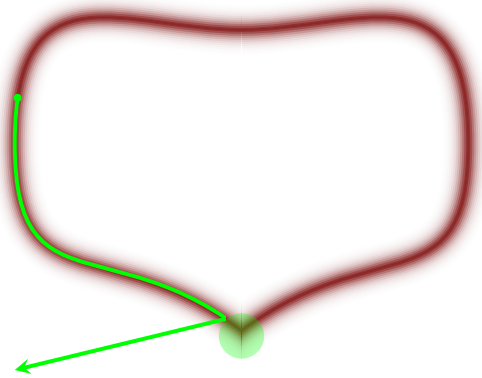

FIG 35. *Neighborhoods of high curvature in the typical set (green) that frustrate geometric ergodicity are also pathological to symplectic integrators, causing them to diverge. This confluence of pathologies is advantageous in practice because we can use the easily-observed divergences to identify the more subtle statistical pathologies.*

is no guarantee that a target distribution will not manifest more subtle pathologies capable of derailing Hamiltonian Monte Carlo, especially as we endeavor towards more and more complex problems.

Still, these diagnostics make Hamiltonian Monte Carlo a uniquely robust method, especially when combined with generic diagnostics like the split $\hat{R}$ statistic with multiple, parallel chains.

7. CONCLUSION

By exploiting the geometry of the typical set, Hamiltonian Monte Carlo generates coherent exploration of smooth target distributions. This effective exploration yields not only better computational efficiency than other Markov chain Monte Carlo algorithms, but also stronger guarantees on the validity of the resulting estimators. Moreover, careful analysis of this geometry facilitates principled strategies for automatically constructing optimal implementations of the method, allowing users to focus their expertise into building better models instead of wrestling with the frustrations of statistical computation. Consequently, Hamiltonian Monte Carlo is uniquely suited to tackling the most challenging problems at the frontiers of applied statistics, as demonstrated by the huge success of tools like Stan (Stan Development Team, 2017).

In hindsight, this success should not be particularly surprising. The ultimate challenge in estimating probabilistic expectations is quantifying the typical set of the target distribution, a set which concentrates near a complex surface in parameter space. What more natural way is there to quantify and then exploit information about a surface than through its geometry?

Continuing to leverage this geometric perspective will be critical to further advancing our

understanding of the Hamiltonian Monte Carlo method and its optimal implementations. This includes everything from improving geometric ergodicity analysis, refining the existing implementation techniques, and motivating the appropriate use of non-Gaussian and non-Euclidean kinetic energies.

Furthermore, techniques from differential geometry may allow us to generalize the principles of Hamiltonian Monte Carlo to other, more challenging computational problems. For example, geometric methods have already generalized coherent exploration to thermodynamic algorithms in *Adiabatic Monte Carlo* (Betancourt, 2014). Incorporating more sophisticated geometric techniques may allow us to extend these ideas to more intricately-structured parameter spaces, such as discrete spaces, tree spaces, and Hilbert spaces.

8. ACKNOWLEDGEMENTS

This conceptual description of Hamiltonian Monte Carlo was refined over three years of frequent speaking engagements coincident with active theoretical research. I am hugely indebted to Mark Girolami, Simon Byrne, and Samuel Livingstone with whom the theoretical work flourished, and the Stan development team with whom the implementations were developed. I also warmly thank Matthew Hoffman, Gareth Roberts, Dan Simpson, Chris Wendl, and everyone who came out to see one of my talks or take the time to ask a question. The manuscript itself benefited from the valuable comments of Ellie Sherrard-Smith, Daniel Lee, Maggie Lieu, Chris Jones, Nathan Sanders, Aki Vehtari, Cole Monnahan, Bob Carpenter, Jonah Sol Gabry, Andrew Gelman, Sidharth Kshatriya, Fabian Dablander, Don van den Bergh, and Nathan Evans.

This was work supported by EPSRC grant EP/J016934/1, a Centre for Research in Statistical Methodology Fellowship, and a 2014 EPRSC NCSML Award for Postdoctoral Research Associate Collaboration.

APPENDIX A: TECHNICAL DETAILS OF PRACTICAL IMPLEMENTATIONS

As discussed in Section 4.1, Hamiltonian systems naturally decompose into a microcanonical distribution over energy level sets and a marginal energy distribution between the energies themselves. Hamiltonian Monte Carlo exploits this structure to generate efficient exploration of the canonical distribution, alternating between exploring a given energy level set and resampling the momenta to generate a random walk over the marginal energy distribution.

In particular, the exploration over the energy level sets is readily accomplished by following the trajectories generated by the Hamiltonian. These trajectories are not only energy preserving, and hence confined to a single energy level set, they are typically ergodic and will explore that entire level set as the trajectories are integrated for longer and longer. More formally, a uniform sample from an ergodic trajectory converges to a sample from the microcanonical distribution.

Unfortunately we cannot implement this idealized method in practice because outside

of a few exceptional systems we cannot generate Hamiltonian trajectories analytically. Instead we have to work with the approximate trajectories given by numerical integrators. Fortunately, Hamiltonian systems admit very powerful symplectic integrators whose numerical errors not only are small but also can be exactly rectified with straightforward probabilistic corrections.

In this appendix I will review the technical details of how the numerical trajectories from symplectic integrators can be utilized to generate samples from the exact microcanonical distribution, first for the case of *static* trajectories of a fixed length and then *dynamic* trajectories that grow until a given termination criterion is met. Finally I will comment on how these implementations relate to the No-U-Turn sampler and Stan.

A.1 Notation

Let $z = (q, p)$ denote a point in phase space. A symplectic integrator generates a numerical trajectory, $\mathfrak{t}$, from any such point by integrating either forwards and backwards for an incremental amount of time, ϵ, reducing all of phase space to the discrete set of points that can be reached by the symplectic integrator.

Given an initial point, z_0, let z_n denote the point reached by integrating forward n times, and z_{-n} the point reached by integrating backwards n times. Example trajectories of length $L = 3$ then include $\mathfrak{t} = \{z_0, z_1, z_2\}$, $\mathfrak{t} = \{z_{-1}, z_0, z_1\}$, and $\mathfrak{t} = \{z_{-2}, z_{-1}, z_0\}$.

I will write the set of all symplectic integrator trajectories of length L that contain the point z as $\mathfrak{T}^L_z$. Similarly, I will denote the set of numerical trajectories of length L that contain the points z and z' as $\mathfrak{T}^L_{z,z'}$, i.e.

$$\mathfrak{T}^L_{z,z'} = \mathfrak{T}^L_z \cap \mathfrak{T}^L_{z'}.$$

A.2 Static Implementations

Symplectic integrators are not exactly energy preserving, causing their numerical trajectories to deviate from the target energy level set. In particular, sampling a state uniformly from any numerical trajectory will not generate a sample from the canonical distribution. This error, however, can be exactly corrected by sampling from the trajectory not uniformly but rather with weights proportional to the desired canonical density function.

The easiest way to reason about any such scheme is sequentially, first by sampling a numerical trajectory that contains the initial point, $\mathbb{T}(\mathfrak{t} \mid z)$, and then sampling a state from that trajectory, $\mathbb{T}(z' \mid \mathfrak{t})$, yielding the joint transition

$$\mathbb{T}(z' \mid z) = \sum_{\mathfrak{t}} \mathbb{T}(z' \mid \mathfrak{t}) \, \mathbb{T}(\mathfrak{t} \mid z),$$

where the sum runs over all numerical trajectories.

A.2.1 Sampling a Trajectory In the static case we consider only the trajectories of length L that contain the initial point, z, in which case $\mathbb{T}(\mathfrak{t} \mid z)$ is supported only on $\mathfrak{T}^L_z$.

In order to ensure a valid correction, this transition from states to trajectories has to exhibit a certain reversibility. Formally we require that the probability of transitions to a trajectory is the same regardless of from which state in that trajectory we might begin,

$$\mathbb{T}(\mathfrak{t} \mid z) = \mathbb{T}(\mathfrak{t} \mid z'),\ \mathfrak{t} \in \mathfrak{T}^{L}_{z,z'}.$$

This has the important implication that

$$\mathbb{I}(z' \in \mathfrak{t})\, \mathbb{T}(\mathfrak{t} \mid z) = \mathbb{I}(z \in \mathfrak{t})\, \mathbb{T}(\mathfrak{t} \mid z),$$

where $\mathbb{I}$ is the indicator function.

In practice this condition is most easily satisfied by uniformly sampling over all of the trajectories that contain the initial point,

$$\mathbb{T}(\mathfrak{t} \mid z) = U\left(\mathfrak{T}^{L}_{z}\right),$$

as $\mathbb{T}(\mathfrak{t} \mid z) = \mathbb{T}(\mathfrak{t} \mid z') = L^{-1}$ if $\mathfrak{T}^{L}_{z,z'} \neq \emptyset$.

A.2.2 Sampling a State Once we have sampled a numerical trajectory, we can generate a sample from the exact canonical distribution with any process that yields transition probabilities proportional to the canonical densities,

$$\begin{aligned} \mathbb{T}(z' \mid \mathfrak{t}) &= \frac{\pi(z')}{\sum_{z'' \in \mathfrak{t}} \pi(z'')} \mathbb{I}(z' \in \mathfrak{t}) \\ &= \frac{e^{-H(z')}}{\sum_{z'' \in \mathfrak{t}} e^{-H(z'')}} \mathbb{I}(z' \in \mathfrak{t}). \end{aligned} \tag{1}$$

If the symplectic integrator were exact, and the numerical trajectories confined to the initial energy level set, then these transition probabilities would reduce to the uniform distribution over the states in the trajectory, as desired. In practice the error in the numerical trajectory induces non-uniform transition probabilities that disfavor deviations towards higher energies.

There are various schemes capable of yielding the desired transition probabilities. For example, we could implement a slice sampler by augmenting the transition with a random variable $u \sim U\left(0, \pi(z)\right)$, and then sampling uniformly from those states in the trajectory satisfying $\pi(z') > u$.

We can also achieve the desired transition probabilities directly, however, by simply drawing from a multinomial distribution over the states in the trajectory with probabilities

$$\mathbb{P}(z') = \frac{\pi(z')}{\sum_{z'' \in \mathfrak{t}} \pi(z'')}.$$

Not only is this approach straightforward to implement, the Rao-Blackwell Theorem establishes that the lack of auxiliary random variables will ensure better performance.

A.2.3 Invariance of the Canonical Distribution Symplectic integrators are able to realize such high practical performance because they exactly preserve volume in phase space. Conveniently, this volume preservation also ensures that we can achieve samples from the exact canonical distribution with any transition that preserves the canonical density,

$$\pi(z) \propto e^{-H(z)}.$$

An explicit calculation shows that the properties laid out above are sufficient to guarantee this invariance,

$$\begin{aligned}
\sum_{z} \mathbb{T}(z'|z)\pi(z) &= \sum_{z} \sum_{\mathfrak{t}} \mathbb{T}(z' \mid \mathfrak{t})\, \mathbb{T}(\mathfrak{t} \mid z)\pi(z) \\
&= \sum_{z} \sum_{\mathfrak{t}} \frac{\pi(z')}{\sum_{z'' \in \mathfrak{t}} \pi(z'')} \mathbb{I}(z' \in \mathfrak{t}) \mathbb{T}(\mathfrak{t} \mid z)\pi(z) \\
&= \sum_{z} \sum_{\mathfrak{t}} \frac{\pi(z')}{\sum_{z'' \in \mathfrak{t}} \pi(z'')} \mathbb{I}(z \in \mathfrak{t}) \mathbb{T}(\mathfrak{t} \mid z')\pi(z) \\
&= \sum_{\mathfrak{t}} \frac{\pi(z')}{\sum_{z'' \in \mathfrak{t}} \pi(z'')} \mathbb{T}(\mathfrak{t} \mid z') \sum_{z} \mathbb{I}(z \in \mathfrak{t})\pi(z) \\
&= \pi\left(z'\right) \sum_{\mathfrak{t}} \frac{1}{\sum_{z'' \in \mathfrak{t}} \pi(z'')} \mathbb{T}(\mathfrak{t} \mid z') \sum_{z \in \mathfrak{t}} \pi(z) \\
&= \pi\left(z'\right) \sum_{\mathfrak{t}} \mathbb{T}(\mathfrak{t} \mid z') \\
&= \pi\left(z'\right).
\end{aligned}$$

A.3 Efficient Static Implementations

The problem with this initial scheme is that it requires us to keep the entire trajectory in memory in order to generate the transition. For static trajectories of length L, this requires keeping L states in memory at any given time, which can become burdensome in high-dimensional problems. We can construct a much more efficient transition, however, by weaving the sampling from $\mathbb{T}(z' \mid \mathfrak{t})$ into the construction of the trajectory, $\mathfrak{t}$, itself.

A.3.1 Uniform Progressive Sampling Instead of sampling a trajectory containing the initial point at once, consider generating a random trajectory sequentially. We begin with a trajectory containing the initial point, $\mathfrak{t}_{\text{old}}$ and then append a new trajectory, $\mathfrak{t}_{\text{new}}$, by randomly integrating either forwards or backwards in time. The union of these two component trajectories gives the complete trajectory, $\mathfrak{t} = \mathfrak{t}_{\text{old}} \cup \mathfrak{t}_{\text{new}}$.

If we had samples from both the old and new trajectories according to (1),

$$z_{\text{old}} \sim \mathbb{T}(z' \mid \mathfrak{t}_{\text{old}}),\ z_{\text{new}} \sim \mathbb{T}(z' \mid \mathfrak{t}_{\text{new}}),$$

then we could generate a sample from the entire trajectory with a Bernoulli process that takes $z = z_{\text{old}}$ with probability p_{old} and $z = z_{\text{new}}$ otherwise (Figure 36), where

$$p_{\text{old}} = \frac{w_{\text{old}}}{w_{\text{old}} + w_{\text{new}}},$$

with $w_{\text{old}} = \sum_{z \in \mathfrak{t}_{\text{old}}} \pi(z)$ and $w_{\text{new}} = \sum_{z \in \mathfrak{t}_{\text{new}}} \pi(z)$.

Formally we have

$$\begin{aligned} \mathbb{T}(z' \mid \mathfrak{t}) &= p_{\text{old}}\, \mathbb{T}(z' \mid \mathfrak{t}_{\text{old}}) + (1 - p_{\text{old}})\, \mathbb{T}(z' \mid \mathfrak{t}_{\text{new}}) \\ &= \frac{w_{\text{old}}}{w_{\text{old}} + w_{\text{new}}} \mathbb{T}(z' \mid \mathfrak{t}_{\text{old}}) + \frac{w_{\text{new}}}{w_{\text{old}} + w_{\text{new}}} \mathbb{T}(z' \mid \mathfrak{t}_{\text{new}}), \end{aligned} \tag{2}$$

which immediately follows from the definition,

$$\begin{aligned} &\frac{w_{\text{old}}}{w_{\text{old}} + w_{\text{new}}} \mathbb{T}(z' \mid \mathfrak{t}_{\text{old}}) + \frac{w_{\text{new}}}{w_{\text{old}} + w_{\text{new}}} \mathbb{T}(z' \mid \mathfrak{t}_{\text{new}}) \\ &\quad = \frac{\sum_{z'' \in \mathfrak{t}_{\text{old}}} \pi(z'')}{\sum_{z'' \in \mathfrak{t}} \pi(z'')} \frac{\pi(z')}{\sum_{z'' \in \mathfrak{t}_{\text{old}}} \pi(z'')} \mathbb{I}(z' \in \mathfrak{t}_{\text{old}}) \\ &\qquad + \frac{\sum_{z'' \in \mathfrak{t}_{\text{new}}} \pi(z'')}{\sum_{z'' \in \mathfrak{t}} \pi(z'')} \frac{\pi(z')}{\sum_{z'' \in \mathfrak{t}_{\text{new}}} \pi(z'')} \mathbb{I}(z' \in \mathfrak{t}_{\text{new}}) \\ &\quad = \frac{\pi(z')}{\sum_{z'' \in \mathfrak{t}} \pi(z'')} \mathbb{I}(z' \in \mathfrak{t}_{\text{old}}) + \frac{\pi(z')}{\sum_{z'' \in \mathfrak{t}} \pi(z'')} \mathbb{I}(z' \in \mathfrak{t}_{\text{new}}) \\ &\quad = \frac{\pi(z')}{\sum_{z'' \in \mathfrak{t}} \pi(z'')} \left(\mathbb{I}(z' \in \mathfrak{t}_{\text{old}}) + \mathbb{I}(z' \in \mathfrak{t}_{\text{new}}) \right) \\ &\quad = \frac{\pi(z')}{\sum_{z'' \in \mathfrak{t}} \pi(z'')} \mathbb{I}(z' \in \mathfrak{t}) \\ &\quad = \mathbb{T}(z' \mid \mathfrak{t}). \end{aligned}$$

This progressive sampling allows us to generate a sample as we build the trajectory itself, keeping only a few states in memory at any given time. For example, starting with the initial point as the active sample we could repeatedly expand the trajectory by integrating one step forward or backwards in time and then update the active sample using the transition above, yielding at once both $\mathfrak{t} \sim \mathbb{T}(\mathfrak{t} \mid z) = U\left(\mathfrak{T}_z^{L+1}\right)$ and $z' \sim \mathbb{T}(z \mid \mathfrak{t})$. This additive expansion scheme also coincides with Neal's windowed sampler when the window length equals the full trajectory length (Neal, 1994).

We can also expand faster by doubling the length of the trajectory at every iteration, yielding a sampled trajectory $\mathfrak{t} \sim \mathbb{T}(\mathfrak{t} \mid z) = U\left(\mathfrak{T}_z^{2L}\right)$ with the corresponding sampled state $z' \sim \mathbb{T}(z' \mid \mathfrak{t})$. In this case both the old and new trajectory components at every iteration are equivalent to the leaves of perfect, ordered binary trees (Figure 37). This allows us to build the new trajectory components recursively, propagating a sample at each step in the recursion using (2) until we have both a new trajectory and a new sample (Figure 38).

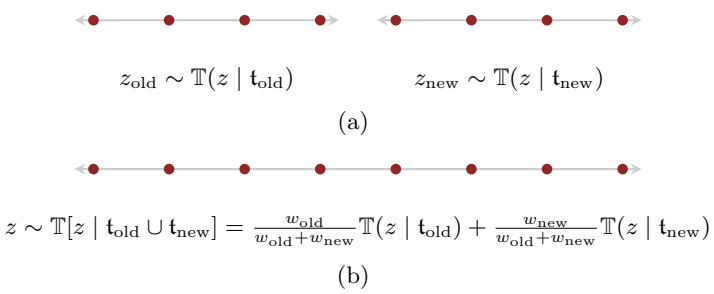

FIG 36. *(a) Given samples from two adjoining numerical trajectories (b) we can generate a sample from their union with a Bernoulli process, effectively mixing the two component transition distributions into the correct joint transition distribution. This allows us to sample from a trajectory progressively during it's construction, transitioning first between the old and the new components and then a sample therein.*

FIG 37. *When the length of a numerical trajectory is a power of 2, $L = 2^D$, the trajectory is equivalent to the leaves of a perfect, ordered binary tree of depth D.*

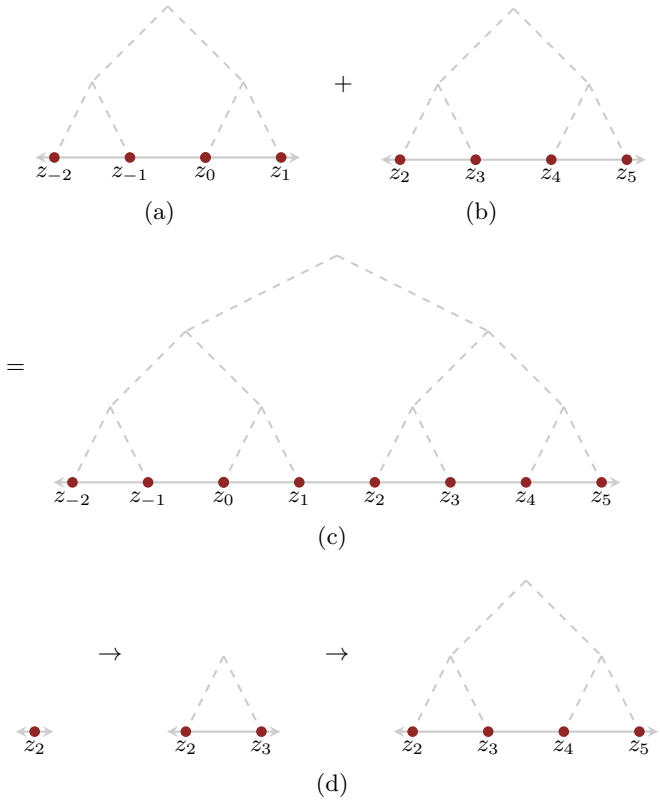

FIG 38. *In multiplicative trajectory expansion we start with (a) an old trajectory component of length* $L = 2^D$ *that contains the initial point,* z_0*, and append (b) a new trajectory component of the same length by randomly integrating either forwards or backwards in time. (c) This yields a trajectory twice as long as the initial trajectory sampled from* $\mathfrak{t} \sim \mathbb{T}(\mathfrak{t} \mid z_0) = U\left(\mathfrak{T}^{2L}_{z_0}\right)$*, with a sampled state* $z' \sim \mathbb{T}(z' \mid \mathfrak{t})$ *generated concurrently from (2). (d) The same process can be also be used to recursively build up the new trajectory component, here initialized from* z_2*, and a corresponding sample* $z_{\text{new}} \sim \mathbb{T}(z' \mid \mathfrak{t}_{\text{new}})$*.*

A.3.2 Biased Progressive Sampling This progressive approach to sampling a state from a random trajectory also provides an opportunity to introduce anti-correlations into the transition and potentially improve performance. Specifically, we can use an alternative transition that satisfies

$$\mathbb{T}(z' \mid \mathfrak{t}) = \min\left(1, \frac{w_{\text{new}}}{w_{\text{old}}}\right) \mathbb{T}(z' \mid \mathfrak{t}_{\text{new}}) + \left(1 - \min\left(1, \frac{w_{\text{new}}}{w_{\text{old}}}\right)\right) \mathbb{T}(z' \mid \mathfrak{t}_{\text{old}}),$$

where $\mathbb{T}(z' \mid \mathfrak{t}_{\text{old}})$ and $\mathbb{T}(z' \mid \mathfrak{t}_{\text{new}})$ are given by (1) as in the uniform progressive sampling approach.

Any such transition favors samples from the new trajectory component and hence biases the transition away from the initial state. When we average over all possible initial states in a given trajectory, however, these repulsions cancel to ensure that we preserve the canonical distribution restricted to the sampled trajectory,

$$\begin{aligned}
\sum_z \mathbb{T}(z' \mid z)\pi(z)\,\mathbb{I}(z \in \mathfrak{t}) &= \sum_z \mathbb{T}(z' \mid z)\pi(z)\,\mathbb{I}(z \in \mathfrak{t}_{\text{old}}) + \sum_z \mathbb{T}(z' \mid z)\pi(z)\,\mathbb{I}(z \in \mathfrak{t}_{\text{new}}) \\
&= \sum_z \mathbb{T}(z' \mid \mathfrak{t}_{\text{old}})\pi(z)\,\mathbb{I}(z \in \mathfrak{t}_{\text{old}}) + \sum_z \mathbb{T}(z' \mid \mathfrak{t}_{\text{new}})\pi(z)\,\mathbb{I}(z \in \mathfrak{t}_{\text{new}}) \\
&= \mathbb{T}(z' \mid \mathfrak{t}_{\text{old}}) \sum_z \pi(z)\,\mathbb{I}(z \in \mathfrak{t}_{\text{old}}) + \mathbb{T}[z' \mid \mathfrak{t}_{\text{new}}] \sum_z \pi(z)\,\mathbb{I}(z \in \mathfrak{t}_{\text{new}}) \\
&= \mathbb{T}(z' \mid \mathfrak{t}_{\text{old}}) w_{\text{old}} + \mathbb{T}(z' \mid \mathfrak{t}_{\text{new}}) w_{\text{new}} \\
&= \quad \min\left(1, \frac{w_{\text{new}}}{w_{\text{old}}}\right) \frac{\pi(z')}{w_{\text{new}}} \mathbb{I}(z' \in \mathfrak{t}_{\text{new}}) w_{\text{old}} \\
&\quad + \left(1 - \min\left(1, \frac{w_{\text{new}}}{w_{\text{old}}}\right)\right) \frac{\pi(z')}{w_{\text{old}}} \mathbb{I}(z' \in \mathfrak{t}_{\text{old}}) w_{\text{old}} \\
&\quad + \min\left(1, \frac{w_{\text{old}}}{w_{\text{new}}}\right) \frac{\pi(z')}{w_{\text{old}}} \mathbb{I}(z' \in \mathfrak{t}_{\text{old}}) w_{\text{new}} \\
&\quad + \left(1 - \min\left(1, \frac{w_{\text{old}}}{w_{\text{new}}}\right)\right) \frac{\pi(z')}{w_{\text{new}}} \mathbb{I}(z' \in \mathfrak{t}_{\text{new}}) w_{\text{new}} \\
&= \quad \min\left(\frac{w_{\text{old}}}{w_{\text{new}}}, 1\right) \pi(z') \mathbb{I}(z' \in \mathfrak{t}_{\text{new}}) \\
&\quad + \left(1 - \min\left(1, \frac{w_{\text{new}}}{w_{\text{old}}}\right)\right) \pi(z') \mathbb{I}(z' \in \mathfrak{t}_{\text{old}}) \\
&\quad + \min\left(\frac{w_{\text{new}}}{w_{\text{old}}}, 1\right) \pi(z') \mathbb{I}(z' \in \mathfrak{t}_{\text{old}}) \\
&\quad + \left(1 - \min\left(1, \frac{w_{\text{old}}}{w_{\text{new}}}\right)\right) \pi(z') \mathbb{I}(z' \in \mathfrak{t}_{\text{new}}) \\
&= \pi(z')\,\mathbb{I}(z' \in \mathfrak{t}_{\text{old}}) + \pi(z')\,\mathbb{I}(z' \in \mathfrak{t}_{\text{new}}) \\
&= \pi(z')\,\mathbb{I}(z' \in \mathfrak{t}).
\end{aligned}$$

A.4 Dynamic Implementations

No matter how efficient we can make a static scheme, it will unfortunately be fundamentally limited. Aside from a few exceptionally simple problems, each energy level set will require a different integration time to achieve the same effective exploration. Some level sets can be surveyed with only short integration times, while others require very long integration times. In order to ensure optimal performance of the Hamiltonian Monte Carlo method we need dynamic implementations that can automatically tune the integration time to approximate uniform exploration across all energy level sets.

Fortunately, the efficient static schemes discussed in Section A.3 can be iterated to achieve a dynamic implementation once we have chosen a criterion for determining when a trajectory has grown long enough to satisfactory explore the corresponding energy level set. We first building an initial trajectory of a given length and then check the termination criterion. If the criterion is not met, we expand the trajectory further and repeat, but if the criterion is met then we return the trajectory and its corresponding sample.

Care must be taken, however, to ensure that such a dynamic scheme does not obstruct the reversibility of the trajectory sampling and hence the desired invariance of the canonical distribution. In this section I will first demonstrate how naive dynamic schemes can frustrate reversibility and what steps we have to take to avoid these problems. With a valid dynamic implementation understood I will then review potential termination criteria.

A.4.1 Maintaining Reversibility The problem with the naive dynamic scheme discussed above is that it can violate the reversibility condition,

$$\mathbb{T}(\mathfrak{t} \mid z) = \mathbb{T}(\mathfrak{t} \mid z'), \, \mathfrak{t} \in \mathfrak{T}^{L}_{z,z'},$$

for the expanded trajectory, and hence the bias the stationary distribution of the resulting Markov chain. In particular, if we initialize from a different point in the final trajectory then the dynamic trajectory expansion might terminate prematurely before reaching the final trajectory, causing $\mathbb{T}(\mathfrak{t} \mid z)$ to vanish for some initial states but not others (Figure 39).

In order to equalize the transition probabilities we have to reject any trajectory expansions that contains certain sub-trajectories satisfying the termination criterion and hence states that would have prematurely terminated if we had instead begun there. For example, if we expand the trajectories additively then we need to check the termination criterion for the sub-trajectories beginning at every state in the old trajectory and ending at the single state in the new trajectory, inducing a cost linear in the size of the old trajectory (Figure 40a). Doing this for each expansion results in a cost quadratic in the final trajectory length.

If we expand the trajectories multiplicatively, however, then we need check only the sub-trajectories equivalent to binary sub-trees of the new trajectory, at a cost just logarithmic in the size of the old trajectory (Figure 40b) and a total cost quadratic only in the log of final trajectory length. Moreover, because the checks occur across sub-trees we can compute them concurrently as we build the new trajectory. If any sub-tree satisfies the termination

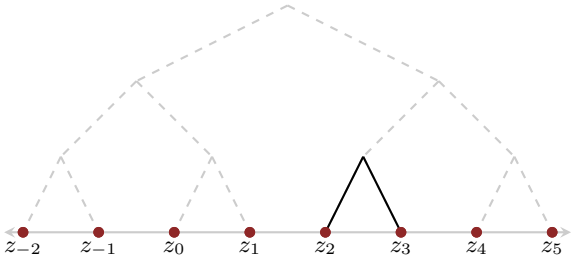

FIG 39. *Naively expanding a trajectory until a dynamic termination criterion is satisfied is not sufficient to ensure reversibility and hence the validity of the resulting Markov chain. When expanding trajectories multiplicatively, for example, if the termination criterion is satisfied by any sub-tree, for example the trajectory beginning at z_2 and ending at z_3, then both $\mathbb{T}(\mathfrak{t} \mid z_2) = 0$ and $\mathbb{T}(\mathfrak{t} \mid z_3) = 0$ despite $\mathbb{T}(\mathfrak{t} \mid z_0) \neq 0$. To avoid this pathology we have to reject any trajectory expansions that contain such pathological sub-trajectories.*

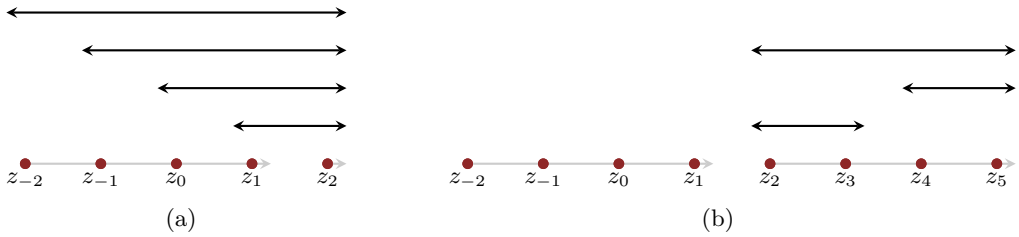

FIG 40. *(a) In an additive expansion scheme we have to check the termination criterion for all sub-trajectories between each point in the old trajectory and the single point in the new trajectory. (b) In a multiplicative expansion scheme, however, we need to check the termination criterion across only the binary sub-trees of the new trajectory.*

criterion prematurely then we can immediately reject the new trajectory without having to build it to completion.

A.4.2 Dynamic Termination Criteria Now we can finally consider explicit termination criteria that can, to varying degrees of success, identify when a trajectory is long enough to yield sufficient exploration of the neighborhood around the current energy level set. In particular, we want to avoid both integrating too short, in which case we would not take full advantage of the Hamiltonian trajectories, and integrating too long, in which case we waste precious computational resources on exploration that yields only diminishing returns.

The first criterion of this form was a heuristic introduced in the No-U-Turn sampler (Hoffman and Gelman, 2014) that considered only the boundaries of a trajectory. Let $z_-(\mathfrak{t})$ and $z_+(\mathfrak{t})$ be the boundaries of the trajectory $\mathfrak{t}$ that can be reached by integrating backwards and forwards in time, respectively (Figure 41). Similarly, denote $q_\pm(\mathfrak{t})$ and $p_\pm(\mathfrak{t})$ as the position and momentum at each boundary. On Euclidean space we can then write the

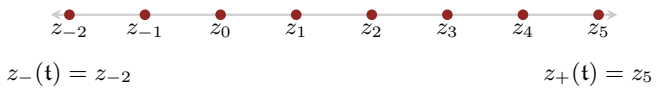

FIG 41. *The No-U-Turn termination criterion considers only the boundaries of a trajectory. The negative boundary, $z_-(\mathrm{t})$, refers to the boundary that can be reached by integrating backwards in time, while the positive boundary, $z_+(\mathrm{t})$ refers to the boundary that can be reached by integrating forwards in time.*

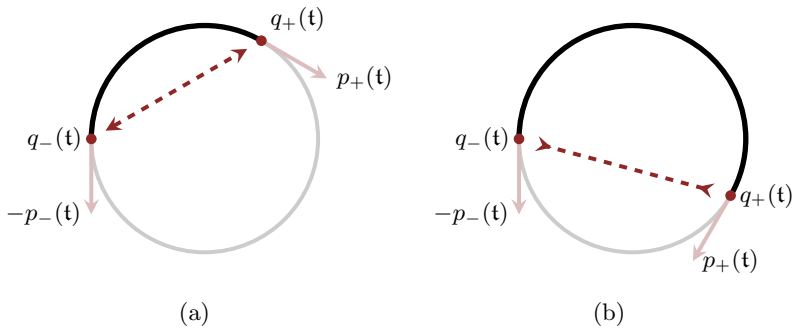

FIG 42. *(a) When the No-U-Turn termination criterion is not satisfied, expanding the trajectory in either direction typically extends the trajectory further across the energy level set (grey) towards unexplored neighborhoods. (b) When the No-U-Turn termination criterion is satisfied, however, further expansion typically contracts the boundaries of the trajectory towards each other and neighborhoods that have already been explored. Stopping when the No-U-Turn termination criterion is just satisfied typically ensures that each trajectory efficiently explores about half of the energy level set. Although this can be too aggressive, it works well empirically and is far superior to any scheme with only a static integration time.*

No-U-Turn termination criterion as

$$\begin{aligned} &p_+(\mathrm{t})^T \cdot (q_+(\mathrm{t}) - q_-(\mathrm{t})) < 0 \\ &\text{AND } p_-(\mathrm{t})^T \cdot (q_-(\mathrm{t}) - q_+(\mathrm{t})) < 0. \end{aligned} \tag{3}$$

This termination criterion is satisfied only when the momentum at both ends of the trajectory are anti-aligned along the line connecting the positions at each boundary. In this case we would expect further integration in either direction to bring the ends of the trajectory closer together, which typically happens only when the trajectory has already expanded across the width of the energy level set (Figure 42).

Unfortunately, the original No-U-Turn termination criterion is well-defined only for Euclidean manifolds where we can rigorously define subtraction between points, and hence is inapplicable for non-Euclidean kinetic energies. Fortunately, however, the criterion can be readily generalized. First note that on a Euclidean manifold

$$q_+(\mathrm{t}) - q_-(\mathrm{t}) = \int_{t=0}^{t=T(\mathrm{t})} \mathrm{d}t \, M^{-1} \cdot p(t),$$

where $T(\mathfrak{t})$ is the integration time needed to reach the positive boundary of the trajectory, $z_+(\mathfrak{t})$, from the negative boundary, $z_+(\mathfrak{t})$. Substituting this into (3), for example, allows us to write the first term of the No-U-Turn termination criterion as

$$p_+(\mathfrak{t})^T \cdot (q_+(\mathfrak{t}) - q_-(\mathfrak{t})) = p_+(\mathfrak{t})^T \cdot M^{-1} \cdot \int_{t=0}^{t=T(\mathfrak{t})} \mathrm{d}t\, p(t) = p_+^\sharp(\mathfrak{t})^T \cdot \rho(\mathfrak{t})$$

where

$$p^\sharp(\mathfrak{t}) \equiv M^{-1} \cdot p(\mathfrak{t})$$

and

$$\rho(\mathfrak{t}) \equiv \int_{t=0(\mathfrak{t})}^{t=T(\mathfrak{t})} \mathrm{d}t\, p(t).$$

Continuing the substituting into the second term, and being careful with the signs, then gives the equivalent termination criterion,

$$p_+^\sharp(\mathfrak{t})^T \cdot \rho(\mathfrak{t}) < 0 \quad \text{AND} \quad p_-^\sharp(\mathfrak{t})^T \cdot \rho(\mathfrak{t}) < 0.$$

This new form is well-defined for any Riemannian manifold and hence defines a proper generalization of the No-U-Turn termination criterion to Riemannian manifolds (Betancourt, 2013b).

Although we can't compute ρ analytically in practice, we can readily approximate it as a discrete sum over the momenta in the numerical trajectory generated by the symplectic integrator,

$$\rho(\mathfrak{t}) \approx \sum_{z \in \mathfrak{t}} p(z).$$

Because of the high accuracy of symplectic integrators, this approximation yields almost identical results as at the original No-U-Turn criterion.

The geometry of the Hamiltonian systems behind Hamiltonian Monte Carlo also motivates another termination criterion that doesn't require any Riemannian structure at all. *Exhaustions* track a quantity inherent to Hamiltonian systems called the virial to determine when an energy level set has been sufficiently explored (Betancourt, 2016a). Unfortunately exhaustions introduce an additional tuning parameter that strongly effects the performance of the resulting implementation. Although careful hand-tuning can yield better performance than implementations that use the No-U-Turn termination criterion, we need to understand how to automatically tune exhalations before they can become a practical competitor.

A.5 The No-U-Turn Sampler and the Current State of Stan

With the hindsight of this analysis, we see that the original No-U-Turn sampler (Hoffman and Gelman, 2014) is a dynamic implementation of Hamiltonian Monte Carlo. In addition to the employing the No-U-Turn termination criterion discussed in Section A.4.2, the No-U-Turn sampler uses a multiplicative expansion of each trajectory and a slice sampler to

sample states from those trajectories. Each new trajectory component is sampled using uniform progressive sampling, but the sample update when appending the new component is generated with biased progressive sampling.

Although Stan (Stan Development Team, 2017) was first developed around this original No-U-Turn sampler, more recent releases have adopted some modifications. In addition to the generalized No-U-Turn termination criterion, the Hamiltonian Monte Carlo implementation in Stan uses multinomial sampling from each trajectory instead of slice sampling, which provides a significant improvement in overall performance.

REFERENCES

Betancourt, M. (2013a). A General Metric for Riemannian Hamiltonian Monte Carlo. In *First International Conference on the Geometric Science of Information* (F. Nielsen and F. Barbaresco, eds.). *Lecture Notes in Computer Science* **8085**. Springer.

Betancourt, M. (2013b). Generalizing the No-U-Turn Sampler to Riemannian Manifolds. *ArXiv e-prints* **1304.1920**.

Betancourt, M. (2014). Adiabatic Monte Carlo. *ArXiv e-prints* **1405.3489**.

Betancourt, M. (2016a). Identifying the Optimal Integration Time in Hamiltonian Monte Carlo. *ArXiv e-prints* **1601.00225**.

Betancourt, M. (2016b). Diagnosing Suboptimal Cotangent Disintegrations in Hamiltonian Monte Carlo. *ArXiv e-prints* **1604.00695**.

Betancourt, M., Byrne, S. and Girolami, M. (2014). Optimizing The Integrator Step Size for Hamiltonian Monte Carlo. *ArXiv e-prints* **1410.5110**.

Betancourt, M. and Girolami, M. (2015). Hamiltonian Monte Carlo for Hierarchical Models. In *Current Trends in Bayesian Methodology with Applications* (U. S. Dipak K. Dey and A. Loganathan, eds.) Chapman & Hall/CRC Press.

Betancourt, M., Byrne, S., Livingstone, S. and Girolami, M. (2014). The Geometric Foundations of Hamiltonian Monte Carlo. *ArXiv e-prints* **1410.5110**.

Bishop, C. M. (2006). *Pattern Recognition and Machine Learning. Information Science and Statistics.* Springer, New York.

Blanes, S., Casas, F. and Sanz-Serna, J. M. (2014). Numerical integrators for the Hybrid Monte Carlo method. *ArXiv e-prints* **1405.3153**.

Brooks, S., Gelman, A., Jones, G. L. and Meng, X.-L., eds. (2011). *Handbook of Markov Chain Monte Carlo.* CRC Press, New York.

Duane, S., Kennedy, A. D., Pendleton, B. J. and Roweth, D. (1987). Hybrid Monte Carlo. *Physics Letters B* **195** 216 - 222.

Fernández-Pendás, M., Akhmatskaya, E. and Sanz-Serna, J. M. (2015). Adaptive multi-stage integrators for optimal energy conservation in molecular simulations. *ArXiv e-prints* **1512.03335**.

Gelman, A., Carlin, J. B., Stern, H. S., Dunson, D. B., Vehtari, A. and Rubin, D. B. (2014). *Bayesian Data Analysis*, third ed. *Texts in Statistical Science Series.* CRC Press, Boca Raton, FL.

Geyer, C. J. (1992). Practical Markov Chain Monte Carlo. *Statistical Science* 473–483.

Girolami, M. and Calderhead, B. (2011). Riemann Manifold Langevin and Hamiltonian Monte Carlo Methods. *Journal of the Royal Statistical Society: Series B (Statistical Methodology)* **73** 123–214.

Hairer, E., Lubich, C. and Wanner, G. (2006). *Geometric Numerical Integration: Structure-Preserving Algorithms for Ordinary Differential Equations.* Springer, New York.

Hastings, W. K. (1970). Monte Carlo Sampling Methods Using Markov Chains and Their Applications. *Biometrika* **57** 97–109.

Hoffman, M. D. and Gelman, A. (2014). The No-U-Turn Sampler: Adaptively Setting Path Lengths in Hamiltonian Monte Carlo. *Journal of Machine Learning Research* **15** 1593–1623.

Holmes, S., Rubinstein-Salzedo, S. and Seiler, C. (2014). Curvature and Concentration of Hamiltonian Monte Carlo in High Dimensions.

Leimkuhler, B. and Reich, S. (2004). *Simulating Hamiltonian Dynamics*. Cambridge University Press, New York.

Livingstone, S., Betancourt, M., Byrne, S. and Girolami, M. (2016). On the Geometric Ergodicity of Hamiltonian Monte Carlo.

MacKay, D. J. C. (2003). *Information Theory, Inference and Learning Algorithms*. Cambridge University Press, New York.

Metropolis, N., Rosenbluth, A. W., Rosenbluth, M. N., Teller, A. H. and Teller, E. (1953). Equation of State Calculations by Fast Computing Machines. *The journal of chemical physics* **21** 1087.

Mira, A., Solgi, R. and Imparato, D. (2013). Zero Variance Markov chain Monte Carlo for Bayesian estimators. *Statistics and Computing* **23** 653–662.

Neal, R. M. (1994). An Improved Acceptance Procedure for the Hybrid Monte Carlo Algorithm. *Journal of Computational Physics* **111** 194–203.

Neal, R. M. (1995). Bayesian Learning for Neural Networks PhD thesis, University of Toronto.

Neal, R. M. (2011). MCMC Using Hamiltonian Dynamics. In *Handbook of Markov Chain Monte Carlo* (S. Brooks, A. Gelman, G. L. Jones and X.-L. Meng, eds.) CRC Press, New York.

Oates, C. J., Girolami, M. and Chopin, N. (2016). Control functionals for Monte Carlo integration. *Journal of the Royal Statistical Society: Series B (Statistical Methodology)*.

Robert, C. P. and Casella, G. (1999). *Monte Carlo Statistical Methods*. Springer New York.

Roberts, G. O. and Rosenthal, J. S. (2004). General State Space Markov Chains and MCMC Algorithms. *Probability Surveys* **1** 20–71.

Stan Development Team (2017). Stan: A C++ Library for Probability and Sampling, Version 2.14.0. http://mc-stan.org/.